

Multiplex-controlled phase gate with qubits distributed in a multi-cavity system

Biaoliang Ye¹, Zhen-Fei Zheng², and Chui-Ping Yang^{1,3*}

¹*Quantum Information Research Center, Shangrao Normal University, Shangrao 334001, China*

²*Key Laboratory of Quantum Information, University of Science and Technology of China, Hefei 230026, China and*

³*Department of Physics, Hangzhou Normal University, Hangzhou 310036, China*

(Dated: June 13, 2018)

We present a way to realize a multiplex-controlled phase gate of $n-1$ control qubits simultaneously controlling one target qubit, with n qubits distributed in n different cavities. This multiqubit gate is implemented by using n qutrits (three-level natural or artificial atoms) placed in n different cavities, which are coupled to an auxiliary qutrit. Here, the two logic states of a qubit are represented by the two lowest levels of a qutrit placed in a cavity. We show that this n -qubit controlled phase gate can be realized using only $2n+2$ basic operations, i.e., the number of required basic operations only increases *linearly* with the number n of qubits. Since each basic operation employs the qutrit-cavity or qutrit-pulse resonant interaction, the gate can be fast implemented when the number of qubits is not large. Numerical simulations show that a three-qubit controlled phase gate, which is executed on three qubits distributed in three different cavities, can be high-fidelity implemented by using a circuit QED system. This proposal is quite general and can be applied to a wide range of physical systems, with atoms, NV centers, quantum dots, or various superconducting qutrits distributed in different cavities. Finally, this method can be applied to implement a multiqubit controlled phase gate with atoms using a cavity. A detailed discussion on implementing a three-qubit controlled phase gate with atoms and one cavity is presented.

PACS numbers: 03.67.Bg, 42.50.Dv, 85.25.Cp

I. INTRODUCTION AND MOTIVATION

Cavity or circuit QED has drawn much attention in the growing field of quantum information processing (QIP). Large-scale QIP will most likely need a large number of qubits, and placing all of them in a single cavity may cause practical problems such as decreasing the qubit-cavity coupling strength and increasing the cavity decay rate. Moreover, when compared to QIP with qubits in a single cavity (Fig. 1), the size of QIP with qubits in multiple cavities can be much larger, since the number $n \times m$ of qubits placed in n cavities is n times the number m of qubits placed in a single cavity provided the number of qubits in each cavity is m . Large-scale QIP may require quantum networks consisting of many cavities, each hosting and coupled to multiple qubits. In such an architecture, manipulation of quantum states will occur not only among qubits in the same cavity, *but also among qubits distributed in different cavities*. Thus, how to implement quantum gates on qubits distributed in different cavities becomes necessary and important.

Multiqubit gates are a crucial element in QIP. Generally speaking, there are two types of important multiqubit gates, which have drawn much attention during the past years. The first type of multiqubit gate consists of multiple control qubits simultaneously controlling on a single target qubit [1,2], while the second type of multiqubit gate contains a single qubit simultaneously controlling multiple target qubits [3,4]. It is well known that these two types of multiqubit gates are of significance in QIP. For instances, they have applications in quantum algorithms [5–7], quantum Fourier transform [1], error correction [8–10], quantum cloning [11], and entanglement preparation [12].

Motivated by the above, the focus of this work is on the direct implementation of the first type of multiqubit gate (i.e., a multi-control-qubit gate with multiple control qubits simultaneously controlling a target qubit) with qubits distributed in a multi-cavity system. It is known that this multiqubit controlled gate can in principle be constructed by using single-qubit and two-qubit basic gates. However, when using the conventional gate-decomposing protocols to construct this multiqubit controlled gate [2,13,14], the number of required single-qubit and two-qubit gates increases drastically with the number of qubits. Thus, the gate implementation becomes very complex, even in the case of assuming a universal single-qubit or two-qubit gate could be realized with a single basic operation. As a result, the gate operation time would be quite long and thus the gate fidelity would be significantly deteriorated by decoherence. Hence, it is worthwhile to seek efficient approaches to realize this type of multi-control-qubit gates.

*Electronic address: yangcp@hznu.edu.cn

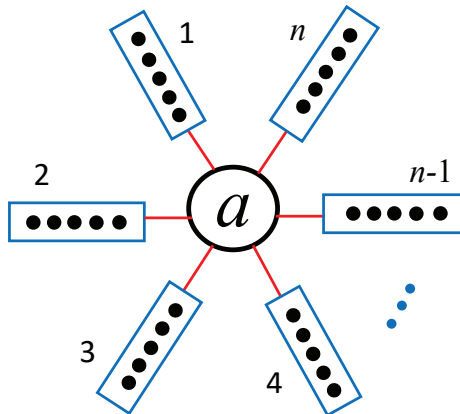


FIG. 1: (Color online) Setup of n cavities connected by a coupler a (a circle at the center). A square represents a cavity, while a dark dot labels a qubit located in each cavity. For clarity, only five qubits in each cavity are shown. In such an architecture, manipulation of quantum states will occur not only among qubits in the same cavity, but also among qubits distributed in different cavities. An important quantum gate among qubits in different cavities is a multiqubit controlled gate with qubits distributed in different cavities. The qubits, which are not involved in the gate operation, can be made to be decoupled to their respective cavities by adjusting the level spacings of qubits or loading the qubits out of the cavities.

To begin with, let us give a brief review on the physical realization of multiqubit quantum gates. For the past years, several schemes for realizing three-qubit Toffoli gates have been proposed with neutral atoms in an optical lattice [15] or hybrid atom-photon qubits [16]. In addition, experimental realization of a controlled phase gate in a three qubit NMR quantum system [17] and a three-qubit Toffoli gate with superconducting qubits [18] has been reported. On the other hand, based on cavity or circuit QED, many theoretical proposals have been presented for directly realizing not only multi-control-qubit gates [19-29] but also multi-target-qubit gates [4,30-33], in various physical qubits. Refs. [19,21-24] discussed how to implement a multi-control-qubit gate with natural or artificial atoms coupled to a single cavity. Refs. [20,25] considered how to realize a multi-control-qubit gate with trapped ions. Refs. [26,27] addressed how to implement a three-qubit control gate with three quantum dots embedded in three spatially-separated cavities with assistance of linear optical devices and photon detections. Refs. [28,29] proposed how to accomplish a multi-control-qubit gate with flying photonic qubits distributed in different cavities coupled to a single qutrit. Refs. [4,30-33] discussed on how to implement a multi-target-qubit gate with natural or artificial atoms placed in or coupled to a single cavity.

Different from previous works [4,19-33], in the following we will propose a method to implement an n -qubit controlled phase gate of $n - 1$ controlled qubits simultaneously controlling a single target qubit, with n qubits in n different cavities coupled to an auxiliary qutrit [Fig. 2(a)]. The two logic states of each qubit here are represented by the two lowest levels of a qutrit (a natural or artificial three-level atom) placed in a cavity [Fig. 2(a)]. As shown below, this proposal has the following advantages: (i) Only one auxiliary qutrit is needed and no other auxiliary system is required; (ii) Since no measurement is needed, the gate realization is deterministic; (iii) Only resonant interaction is used, thus the gate operation can be performed fast for a small number of qubits; and (iv) Because of only $2n + 2$ basic operations are needed, the number of basic operations only increases *linearly* with the number n of qubits; thus the gate procedure is significantly simplified when compared with the conventional gate-decomposing protocols. To the best of our knowledge, this proposal was not reported before.

Finally, it is noted that this method can be applied to implement a multiqubit controlled phase gate with atoms using a cavity. As an example, we will explicitly show how to use the present method to implement a three-qubit controlled phase gate with atoms by loading atoms into or moving atoms out of a cavity.

We stress that the main purpose of this work is on the implementation of a multiqubit controlled gate with qubits distributed in a multi-cavity system instead of a single cavity. As discussed at the beginning, implementing quantum gates on qubits distributed in different cavities is important in large-scale QIP.

This paper is organized as follows. In Sec. II, we review the basic theory. In Sec. III, we explicitly show how to realize a three-qubit controlled phase gate with three qutrits distributed in three different cavities. In Sec. IV, we then discuss how the method can be generalized to implement a n -qubit controlled phase gate with n qutrits distributed in n different cavities. In Sec. V, based on a circuit QED system, we discuss the experimental feasibility of implementing the proposed gate for a three-qubit case. In Sec. VI, we show how to apply the method to realize a

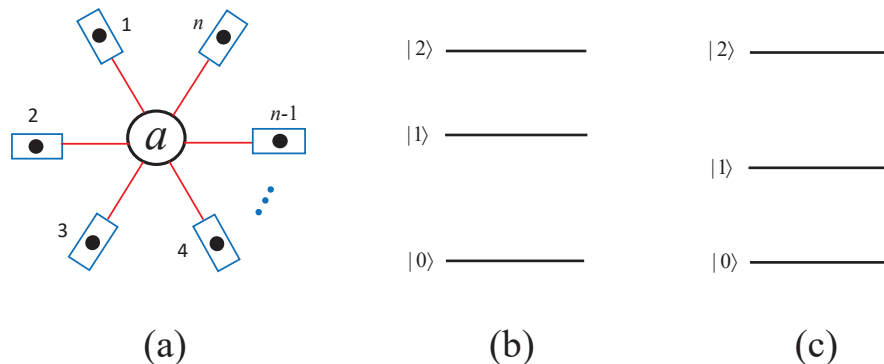


FIG. 2: (Color online) (a) Diagram of a coupler qutrit a (a circle at the center) and n cavities ($1, 2, \dots, n$) each hosting a qutrit. A square represents a cavity, while a dark dot labels a qutrit placed in each cavity. (b) A qutrit with three levels $|0\rangle$, $|1\rangle$ and $|2\rangle$, for which the level spacing between the upper two levels is smaller than that between the two lowest levels. (c) A qutrit, whose level spacing between the upper two levels is greater than that between the two lowest levels. As shown in next section, the $|0\rangle \leftrightarrow |1\rangle$ and $|1\rangle \leftrightarrow |2\rangle$ transitions are required by the gate implementation while the $|0\rangle \leftrightarrow |2\rangle$ transition is not necessary. Note that the level structure in (b) applies to natural atoms, quantum dots, superconducting phase, transmon, and Xmon qutrits; while the level structure in (c) is available in superconducting charge qutrits, flux qutrits, nitrogen-vacancy centers, etc.

three-qubit controlled phase gate with atoms using one cavity. A concluding summary is given in Sec. VII.

II. BASIC THEORY

Our multi-qubit gate is realized with a setup illustrated in Fig. 2(a), where all cavities are coupled to an auxiliary qutrit and each cavity hosts a qutrit. The three levels of each qutrit are denoted as $|0\rangle$, $|1\rangle$ and $|2\rangle$, respectively [Fig. 2(b) and Fig. 2(c)]. As an example, our following presentation starts with qutrits having the level structure depicted in Fig. 2(b). However, we stress that the method presented below for the gate implementation can directly apply to the qutrits with the level structures shown in Fig. 2(c), because for this type of level structure the required Hamiltonians given below can also be obtained.

The qutrit located in cavity l is labelled as qutrit l ($l = 1, 2, \dots, n$), while the auxiliary qutrit, which is coupled to the n cavities, is denoted as qutrit a . As shown in next section, the gate implementation requires: (i) A classical pulse resonantly interacting with the $|1\rangle \leftrightarrow |2\rangle$ transition for each of qutrits ($2, 3, \dots, n$); (ii) Each cavity resonantly interacting with the $|0\rangle \leftrightarrow |1\rangle$ transition of qutrit a ; and (iii) Each cavity simultaneously and resonantly interacting with the $|0\rangle \leftrightarrow |1\rangle$ transition of two qutrits (i.e., qutrit a and qutrit l in cavity l). In the following, we will give a brief introduction to the state evolution under these types of interaction.

A. Qutrit driven by a classical pulse

Let us consider that a classical pulse is applied to qutrit l ($l = 2, 3, \dots, n$). It can be shown that if the pulse is resonant with the $|1\rangle \leftrightarrow |2\rangle$ transition but far-off resonant with (decoupled from) the $|0\rangle \leftrightarrow |1\rangle$ transition and the $|0\rangle \leftrightarrow |2\rangle$ transition of the qutrit [Fig. 3(a)], then the interaction Hamiltonian in the interaction picture and after making a rotating-wave approximation (RWA) is given by

$$H_{I_1} = \hbar (\Omega_l e^{i\phi_l} |1\rangle_l \langle 2| + \text{h.c.}), \quad (1)$$

where ϕ_l and Ω_l are the initial phase and the Rabi frequency of the pulse, respectively. From the Hamiltonian (1), it is straightforward to show that a pulse of duration t results in the following rotation

$$\begin{aligned} |1\rangle_l &\rightarrow \cos \Omega_l t |1\rangle_l - ie^{-i\phi_l} \sin \Omega_l t |2\rangle_l, \\ |2\rangle_l &\rightarrow -ie^{i\phi_l} \sin \Omega_l t |1\rangle_l + \cos \Omega_l t |2\rangle_l. \end{aligned} \quad (2)$$

B. Qutrit coupled to a single cavity

Consider qutrit a coupled to cavity l ($l = 1, 2, \dots, n$). Suppose that cavity l is resonantly coupled to the $|0\rangle \leftrightarrow |1\rangle$ transition while highly detuned (decoupled) from the transitions between other levels of the qutrit [Fig. 3(b)]. Under this consideration, the interaction Hamiltonian in the interaction picture and after the RWA, can be written as

$$H_{I_2} = \hbar (g_l a_l^\dagger |0\rangle_a \langle 1| + \text{h.c.}), \quad (3)$$

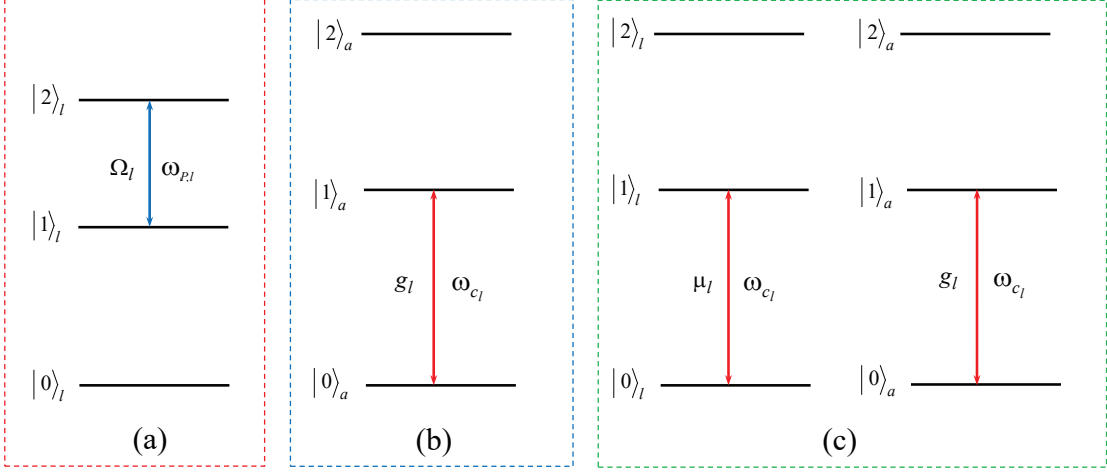


FIG. 3: (Color online) (a) Illustration of a classical pulse resonant with the $|1\rangle \leftrightarrow |2\rangle$ transition of qutrit l . Here, Ω_l is the pulse Rabi frequency. (b) Illustration of cavity l resonant with the $|0\rangle \leftrightarrow |1\rangle$ transition of qutrit a , with a coupling constant g_l . (c) Illustration of cavity l simultaneously resonant with the $|0\rangle \leftrightarrow |1\rangle$ transition of qutrits l and a , with a coupling constant μ_l for qutrit l and a coupling constant g_l for qutrit a . Note that the level structure of qutrit l in (a) is different from that in (b) and (c), because qutrit l in (a) is decoupled from cavity l during the pulse while the level spacings of qutrits in (b) and (c) are adjusted such that the $|0\rangle \leftrightarrow |1\rangle$ transition is resonant with cavity l . Each horizontal line represents the energy level of qutrit l or qutrit a . A blue double-arrow vertical line in (a) represents the frequency $\omega_{p,l}$ of the pulse applied to qutrit l , while a red double-arrow vertical line in (b) and (c) represents the frequency ω_{c_l} of cavity l .

where a_l^+ (a_l) is the creation (annihilation) operator of cavity l while g_l is the coupling constant between cavity l and the $|0\rangle \leftrightarrow |1\rangle$ transition of qutrit a .

Under the Hamiltonian (3), one can obtain the following state evolution:

$$\begin{aligned} |0\rangle_a |0\rangle_{c_l} &\rightarrow |0\rangle_a |0\rangle_{c_l}, \\ |1\rangle_a |0\rangle_{c_l} &\rightarrow -i \sin g_l t |0\rangle_a |1\rangle_{c_l} + \cos g_l t |1\rangle_a |0\rangle_{c_l}, \end{aligned} \quad (4)$$

where $|0\rangle_{c_l}$ is the vacuum state of cavity l while $|1\rangle_{c_l}$ is the single-photon state of cavity l .

C. Two qutrits coupled to a single cavity

Consider two qutrits l and a coupled to cavity l ($l = 1, 2, \dots, n$). Suppose that the cavity is resonantly coupled to the $|0\rangle \leftrightarrow |1\rangle$ transition but highly detuned (decoupled) from the transitions between other levels of each qutrit [Fig. 3(c)]. Under this consideration, the interaction Hamiltonian in the interaction picture and after the RWA can be written as

$$H_{I_3} = \hbar (\mu_l a_l^+ |0\rangle_l \langle 1| + \text{h.c.}) + \hbar (g_l a_l^+ |0\rangle_a \langle 1| + \text{h.c.}), \quad (5)$$

where μ_l (g_l) is the coupling constant between the cavity mode and the $|0\rangle \leftrightarrow |1\rangle$ transition of qutrit l (qutrit a).

Assume $\mu_l = g_l$. This condition can be readily satisfied, because the coupling strength μ_l can be adjusted by varying the position of qutrit l in cavity l . For solid-state qutrits (e.g., superconducting qutrits or quantum dots), the condition can also be met by adjusting the coupling strength g_l through varying the coupling element (e.g., capacitance or inductance) between qutrit a and cavity l . Thus, under the Hamiltonian (5), one can obtain the following state evolution:

$$\begin{aligned} |0\rangle_l |0\rangle_a |0\rangle_{c_l} &\rightarrow |0\rangle_l |0\rangle_a |0\rangle_{c_l}, \\ |0\rangle_l |1\rangle_a |0\rangle_{c_l} &\rightarrow \frac{1}{2} \left(1 + \cos \sqrt{2} g_l t \right) |0\rangle_l |1\rangle_a |0\rangle_{c_l} - i \frac{\sqrt{2}}{2} \sin \sqrt{2} g_l t |0\rangle_l |0\rangle_a |1\rangle_{c_l} \\ &\quad - \frac{1}{2} \left(1 - \cos \sqrt{2} g_l t \right) |1\rangle_l |0\rangle_a |0\rangle_{c_l}. \end{aligned} \quad (6)$$

The results (2), (4), and (6) presented above will be employed for the gate realization, as shown in the next section.

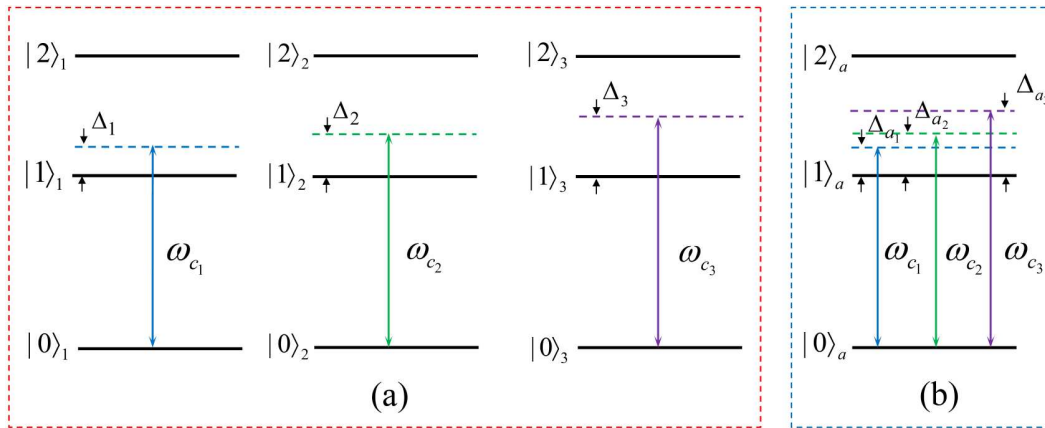


FIG. 4: (Color online) (a) Decoupling of qutrits (1, 2, 3) from their respective cavities before the gate operation (from left to right). Here, Δ_l is a large detuning between the frequency ω_{c_l} of cavity l and the $|0\rangle \leftrightarrow |1\rangle$ transition frequency of qutrit l ($l = 1, 2, 3$), which represents that cavity l is far-off resonant with (decoupled from) the $|0\rangle \leftrightarrow |1\rangle$ transition of qutrit l . (b) Decoupling of qutrit a from three cavities before the gate operation. Here, Δ_{a_l} is a large detuning between the frequency ω_{c_l} of cavity l and the $|0\rangle \leftrightarrow |1\rangle$ transition frequency of qutrit a ($l = 1, 2, 3$), which represents that cavity l is far-off resonant with (decoupled from) $|0\rangle \leftrightarrow |1\rangle$ transition of qutrit a . Because the $|1\rangle \leftrightarrow |2\rangle$ level spacing is smaller than the $|0\rangle \leftrightarrow |1\rangle$ level spacing, there is a *larger* detuning between the frequency of cavity l and the $|1\rangle \leftrightarrow |2\rangle$ transition frequency of qutrits l and a . Hence, cavity l is automatically far-off resonant with (or decoupled from) the $|1\rangle \leftrightarrow |2\rangle$ transition of qutrits l and a . In addition, the coupling of cavity l with the $|0\rangle \leftrightarrow |2\rangle$ transition of qutrits l and a is negligible because the $|0\rangle \leftrightarrow |2\rangle$ level spacing is much greater than the $|0\rangle \leftrightarrow |1\rangle$ level spacing. For simplicity, we consider each qutrit is identical, resulting in $\Delta_l = \Delta_{a_l}$. During the gate operation, we need to bring the $|0\rangle \leftrightarrow |1\rangle$ transition of qutrit a on resonance with cavity l , corresponding to $\Delta_{a_l} = 0$ ($l = 1, 2, 3$). In addition, we need to bring the $|0\rangle \leftrightarrow |1\rangle$ transition of both qutrit l and qutrit a on resonance with cavity l , corresponding to $\Delta_l = \Delta_{a_l} = 0$ ($l = 1, 2, 3$).

III. MULTI-QUBIT CONTROLLED PHASE GATE

To begin with, it should be mentioned that the two logic states 0 and 1 of a qubit are represented by the two lowest levels $|0\rangle$ and $|1\rangle$ of a qutrit. Throughout this paper, qubit l in cavity l corresponds to qutrit l placed in cavity l ($l = 1, 2, \dots, n$). Namely, the n qubits (1, 2, ..., n) below, which are distributed in n different cavities, correspond to the n qutrits (1, 2, ..., n) placed in n different cavities, respectively. In this section, we will first show how to implement a three-qubit controlled phase gate with three qubits distributed in three different cavities, and then give a discussion on the realization of an n -qubit controlled phase gate with n qubits distributed in n different cavities.

A. Implementing a three-qubit controlled phase gate

For three qubits, there are a total number of eight computational basis states, denoted by $|000\rangle, |001\rangle, \dots, |111\rangle$, respectively. A three-qubit controlled phase gate is described by $|000\rangle \rightarrow |000\rangle, |001\rangle \rightarrow |001\rangle, |010\rangle \rightarrow |010\rangle, |011\rangle \rightarrow |011\rangle, |100\rangle \rightarrow |100\rangle, |101\rangle \rightarrow |101\rangle, |110\rangle \rightarrow |110\rangle, |111\rangle \rightarrow -|111\rangle$, which implies that if and only if the two control qubits (the first two qubits) are in the state $|1\rangle$, a phase flip happens to the state $|1\rangle$ of the target qubit (the last qubit) but nothing happens otherwise.

Let us return to the setup shown in Fig. 2(a). For the three-qubit case (i.e., $n = 3$), Fig. 2(a) consists three cavities (1, 2, 3) each hosting a qutrit and coupled to an auxiliary qutrit a . Initially, the three qutrits (1, 2, 3) distributed in the three cavities are decoupled from their respective cavities [Fig. 4(a)], qutrit a is decoupled from all cavities [Fig. 4(b)], and each cavity is in the vacuum state. The 3-qubit controlled phase gate described above can be implemented by the following eight steps of operation, which are described as follows.

Step 1: Apply a classical pulse to each of qutrits (2, 3), which has an initial phase $-\pi/2$ and is resonant with the $|1\rangle \leftrightarrow |2\rangle$ transition. The Rabi frequency of the pulse applied to qutrit l is Ω_l ($l = 2, 3$). After an interaction time $\tau_1 = \pi / (2\Omega_l)$, the state $|1\rangle$ of qutrit l changes to $|2\rangle$ according to Eq. (2). Because of the level spacings of each qutrit being not adjusted (Fig. 4), each qutrit is decoupled from its cavity during the pulse.

Step 2: Bring the $|0\rangle \leftrightarrow |1\rangle$ transition of qutrits 1 and a to resonance with cavity 1 for an interaction time $\tau_2 = \pi / (\sqrt{2}g_1)$ (Fig. 4 with $\Delta_1 = \Delta_{a_1} = 0$), resulting in the state transformation $|1\rangle_1 |0\rangle_a |0\rangle_{c_1} \rightarrow -|0\rangle_1 |1\rangle_a |0\rangle_{c_1}$ according to Eq. (6).

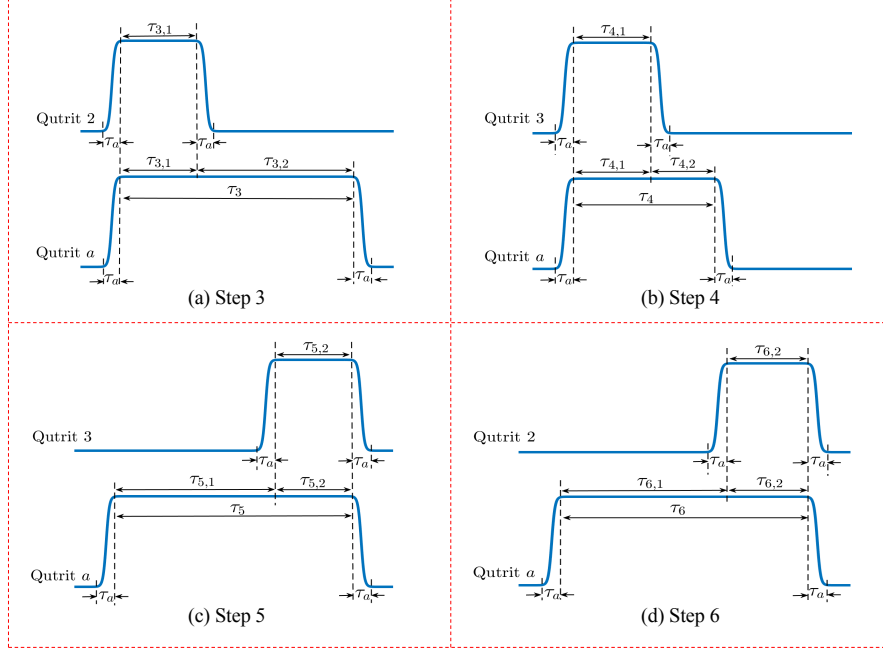


FIG. 5: (Color online) (a) Sequence of operations for step 3. The top figure corresponds to qutrit 2 while the bottom figure corresponds to qutrit a . (b) Sequence of operations for step 4. The top and bottom figures correspond to qutrit 3 and qutrit a , respectively. (c) Sequence of operations for step 5. The top figure corresponds to qutrit 3 while the bottom figure corresponds to qutrit a . (d) Sequence of operations for step 6. The top and bottom figures correspond to qutrit 2 and qutrit a , respectively. Here, $\tau_{k,1}$, $\tau_{k,2}$, and τ_k (with $k = 3, 4, 5, 6$) are the qutrit-cavity interaction times, as described in the text; while τ_a is the typical time required to adjust the qutrit level spacings. Note that the operations in (a)–(d) are performed from left to right.

Step 3: Bring the $|0\rangle \leftrightarrow |1\rangle$ transition of qutrits 2 and a to resonance with cavity 2 for an interaction time $\tau_{3,1} = \pi / (\sqrt{2}g_2)$ (Fig. 4 with $\Delta_2 = \Delta_{a_2} = 0$), resulting in $|0\rangle_2 |1\rangle_a |0\rangle_{c_2} \rightarrow -|1\rangle_2 |0\rangle_a |0\rangle_{c_2}$ according to Eq. (6). Then turn off the interaction between qutrit 2 and cavity 2 such that the state $-|1\rangle_2 |0\rangle_a |0\rangle_{c_2}$ remains unchanged, while let qutrit a continue resonantly interacting with cavity 2 for an additional interaction time $\tau_{3,2} = 2\pi/g_2 - \pi / (\sqrt{2}g_2)$ (Fig. 4 with $\Delta_2 \neq 0$ but $\Delta_{a_2} = 0$). After an interaction time $\tau_3 = \tau_{3,1} + \tau_{3,2} = 2\pi/g_2$, the state $|1\rangle_a |0\rangle_{c_2}$ remains unchanged according to Eq. (4). The operation sequence for this step of operation is illustrated in Fig. 5(a).

Step 4: Bring the $|0\rangle \leftrightarrow |1\rangle$ transition of qutrits 3 and a to resonance with cavity 3 for an interaction time $\tau_{4,1} = \pi / (\sqrt{2}g_3)$ (Fig. 4 with $\Delta_3 = \Delta_{a_3} = 0$), resulting in $|0\rangle_3 |1\rangle_a |0\rangle_{c_3} \rightarrow -|1\rangle_3 |0\rangle_a |0\rangle_{c_3}$ according to Eq. (6). Then, turn off the interaction between qutrit 3 and cavity 3 such that the state $-|1\rangle_3 |0\rangle_a |0\rangle_{c_3}$ remains unchanged, while let qutrit a continue resonantly interacting with cavity 3 for an additional interaction time $\tau_{4,2} = \pi/g_3 - \pi / (\sqrt{2}g_3)$ (Fig. 4 with $\Delta_3 \neq 0$ but $\Delta_{a_3} = 0$). After an interaction time $\tau_4 = \tau_{4,1} + \tau_{4,2} = \pi/g_3$, the state $|1\rangle_a |0\rangle_{c_3}$ becomes $-|1\rangle_a |0\rangle_{c_3}$ according to Eq. (4). The operation sequence for this step of operation is illustrated in Fig. 5(b).

Step 5: Bring the $|0\rangle \leftrightarrow |1\rangle$ transition of qutrit a to resonance with cavity 3 for an interaction time $\tau_{5,1} = 2\pi/g_3 - \pi / (\sqrt{2}g_3)$ (Fig. 4 with $\Delta_{a_3} = 0$). Then, let qutrit a continue resonantly interacting with cavity 3 and bring the $|0\rangle \leftrightarrow |1\rangle$ transition of qutrit 3 to resonance with cavity 3 for an interaction time $\tau_{5,2} = \pi / (\sqrt{2}g_3)$ (Fig. 4 with $\Delta_3 = \Delta_{a_3} = 0$). After the interaction time $\tau_{5,2}$, we have the state transformation $|1\rangle_3 |0\rangle_a |0\rangle_{c_3} \rightarrow -|0\rangle_3 |1\rangle_a |0\rangle_{c_3}$ according to Eq. (6), while after an interaction time $\tau_5 = \tau_{5,1} + \tau_{5,2} = 2\pi/g_3$ the state $|1\rangle_a |0\rangle_{c_3}$ remains unchanged according to Eq. (4). The operation sequence for this step of operation is illustrated in Fig. 5(c).

Step 6: Bring the $|0\rangle \leftrightarrow |1\rangle$ transition of qutrit a to resonance with cavity 2 for an interaction time $\tau_{6,1} = 2\pi/g_2 - \pi / (\sqrt{2}g_2)$ (Fig. 4 with $\Delta_{a_2} = 0$). Then, let qutrit a continue resonantly interacting with cavity 2 and bring the $|0\rangle \leftrightarrow |1\rangle$ transition of qutrit 2 to resonance with cavity 2 for an interaction time $\tau_{6,2} = \pi / (\sqrt{2}g_2)$ (Fig. 4 with $\Delta_2 = \Delta_{a_2} = 0$). After the interaction time $\tau_{6,2}$, one has the state transformation $|1\rangle_2 |0\rangle_a |0\rangle_{c_2} \rightarrow -|0\rangle_2 |1\rangle_a |0\rangle_{c_2}$ according to Eq. (6), while after an interaction time $\tau_6 = \tau_{6,1} + \tau_{6,2} = 2\pi/g_2$ the state $|1\rangle_a |0\rangle_{c_2}$ remains unchanged according to Eq. (4). The operation sequence for this step of operation is illustrated in Fig. 5(d).

Step 7: Bring the $|0\rangle \leftrightarrow |1\rangle$ transition of qutrits 1 and a to resonance with cavity 1 for an interaction time

$\tau_7 = \pi/(\sqrt{2}g_1)$ (Fig. 4 with $\Delta_1 = \Delta_{a_1} = 0$), resulting in the state transformation $|0\rangle_1|1\rangle_a|0\rangle_{c_1} \rightarrow -|1\rangle_1|0\rangle_a|0\rangle_{c_1}$ according to Eq. (6).

Step 8: Bring the $|0\rangle \leftrightarrow |1\rangle$ transition of each qutrit to off-resonance with its cavity or cavities (Fig. 4 with non-zero detunings), such that the qutrit system is decoupled from the cavity system. Then, apply a classical pulse to each of qutrits (2, 3), which has an initial phase $\pi/2$ and is resonant with the $|1\rangle \leftrightarrow |2\rangle$ transition of the qutrits. The Rabi frequency of the pulse applied to qutrit l is Ω_l ($l = 2, 3$). After a pulse duration $\tau_8 = \pi/(2\Omega_l)$, the state $|2\rangle$ of qutrit l changes to $|1\rangle$ according to Eq. (2).

One can check that the states of the whole system after each step of the above operation are summarized below:

$$\begin{array}{ccc}
\begin{array}{l} |100\rangle|0\rangle_a|0\rangle_c \\ |101\rangle|0\rangle_a|0\rangle_c \\ |110\rangle|0\rangle_a|0\rangle_c \\ |111\rangle|0\rangle_a|0\rangle_c \end{array} & \xrightarrow{\text{Step 1}} & \begin{array}{l} |100\rangle|0\rangle_a|0\rangle_c \\ |102\rangle|0\rangle_a|0\rangle_c \\ |120\rangle|0\rangle_a|0\rangle_c \\ |122\rangle|0\rangle_a|0\rangle_c \end{array} & \xrightarrow{\text{Step 2}} & \begin{array}{l} -|000\rangle|1\rangle_a|0\rangle_c \\ -|002\rangle|1\rangle_a|0\rangle_c \\ -|020\rangle|1\rangle_a|0\rangle_c \\ -|022\rangle|1\rangle_a|0\rangle_c \end{array} \\
\begin{array}{l} |010\rangle|0\rangle_a|0\rangle_c \\ |012\rangle|0\rangle_a|0\rangle_c \\ -|020\rangle|1\rangle_a|0\rangle_c \\ -|022\rangle|1\rangle_a|0\rangle_c \end{array} & \xrightarrow{\text{Step 3}} & \begin{array}{l} |010\rangle|0\rangle_a|0\rangle_c \\ |012\rangle|0\rangle_a|0\rangle_c \\ |021\rangle|0\rangle_a|0\rangle_c \\ |022\rangle|1\rangle_a|0\rangle_c \end{array} & \xrightarrow{\text{Step 4}} & \begin{array}{l} |010\rangle|0\rangle_a|0\rangle_c \\ |012\rangle|0\rangle_a|0\rangle_c \\ -|020\rangle|1\rangle_a|0\rangle_c \\ |022\rangle|1\rangle_a|0\rangle_c \end{array} & \xrightarrow{\text{Step 5}} & \begin{array}{l} |010\rangle|0\rangle_a|0\rangle_c \\ |012\rangle|0\rangle_a|0\rangle_c \\ -|020\rangle|1\rangle_a|0\rangle_c \\ |022\rangle|1\rangle_a|0\rangle_c \end{array} \\
\begin{array}{l} -|000\rangle|1\rangle_a|0\rangle_c \\ -|002\rangle|1\rangle_a|0\rangle_c \\ -|020\rangle|1\rangle_a|0\rangle_c \\ |022\rangle|1\rangle_a|0\rangle_c \end{array} & \xrightarrow{\text{Step 6}} & \begin{array}{l} |100\rangle|0\rangle_a|0\rangle_c \\ |102\rangle|0\rangle_a|0\rangle_c \\ |120\rangle|0\rangle_a|0\rangle_c \\ -|122\rangle|0\rangle_a|0\rangle_c \end{array} & \xrightarrow{\text{Step 7}} & \begin{array}{l} |100\rangle|0\rangle_a|0\rangle_c \\ |101\rangle|0\rangle_a|0\rangle_c \\ |110\rangle|0\rangle_a|0\rangle_c \\ -|111\rangle|0\rangle_a|0\rangle_c \end{array} & \xrightarrow{\text{Step 8}} & \begin{array}{l} |100\rangle|0\rangle_a|0\rangle_c \\ |101\rangle|0\rangle_a|0\rangle_c \\ |110\rangle|0\rangle_a|0\rangle_c \\ -|111\rangle|0\rangle_a|0\rangle_c \end{array} \end{array} \quad (7)
\end{array}$$

where $|ijk\rangle$ is abbreviation of the state $|i\rangle_1|j\rangle_2|k\rangle_3$ of qubits (1, 2, 3) with $i, j, k \in \{0, 1, 2\}$ while $|0\rangle_c$ is abbreviation of the state $|0\rangle_{c_1}|0\rangle_{c_2}|0\rangle_{c_3}$ of cavities (1, 2, 3).

On the other hand, it is obvious that the following states of the system

$$|000\rangle|0\rangle_a|0\rangle_c, |001\rangle|0\rangle_a|0\rangle_c, |010\rangle|0\rangle_a|0\rangle_c, |011\rangle|0\rangle_a|0\rangle_c \quad (8)$$

remain unchanged during the entire operation. This is because: the state $|1\rangle$ of each of qutrits 2 and 3 changes to the state $|2\rangle$ after applying the pulses (step 1); no photon was emitted to the cavities during each step of operations above, when each qutrit is in the state $|0\rangle$ or $|2\rangle$ (steps 2-7); and the state $|2\rangle$ of each of qutrits 2 and 3 changes back to the state $|1\rangle$ after applying the pulses (step 8). Thus, we can conclude from Eq. (7) that the three-qubit controlled phase gate was realized with two controlled qubits (1, 2) distributed in two different cavities (1, 2), as well as the target qubit 3 in cavity 3 after the above process.

B. Implementing an n -qubit controlled phase gate

A n -qubit controlled phase gate of n qubits (1, 2, ..., n) is defined by the following transformation

$$|i_1i_2\dots i_n\rangle \rightarrow (-1)^{i_1 \times i_2 \times \dots \times i_n} |i_1i_2\dots i_l\dots i_n\rangle, \quad (9)$$

where subscript l indicates qubit l , $i_l \in \{0, 1\}$, and $|i_1i_2\dots i_l\dots i_n\rangle$ is a n -qubit computational basis state. For n qubits, there exist 2^n computational basis states, forming a set of complete orthogonal bases in a 2^n -dimensional Hilbert space of the n qubits. Eq. (9) implies that only when the $n-1$ control qubits (the first $n-1$ qubits) are all in the state $|1\rangle$, the state $|1\rangle$ of the target qubit (the last qubit) undergoes a phase flip, i.e., $|11\dots 1\rangle \rightarrow -|11\dots 1\rangle$, while nothing happens to all other $2^n - 1$ computational basis states. In the following, we will discuss how this multi-qubit controlled phase gate can be achieved with n qutrits distributed in different cavities.

Let us now consider a setup shown in Fig. 2(a), where each cavity hosts a qutrit and coupled to an auxiliary qutrit a . Suppose that qutrits (1, 2, ..., n), distributed in the n cavities, are initially decoupled from their respective cavities and qutrit a is decoupled from all cavities (Fig. 6). Each cavity is initially in the vacuum state. Examining the above operations for the three-qubit controlled phase gate carefully, we find that the n -qubit controlled phase gate (9) can be obtained with each cavity returning to the original vacuum state, by the following sequence of operators

$$U = U_{2n+2} \otimes U_{2n+1} \otimes \left(\prod_{l=1}^{n-1} U_{n+l+1} \right) \otimes U_{n+1} \otimes \left(\prod_{l=2}^{n-1} U_{l+1} \right) \otimes U_2 \otimes U_1, \quad (10)$$

where $U_1, U_2, U_{l+1}, U_{n+1}, U_{n+l+1}, U_{2n+1}$, and U_{2n+2} represent unitary operators. The state transformations arising from the unitary operators are described below:

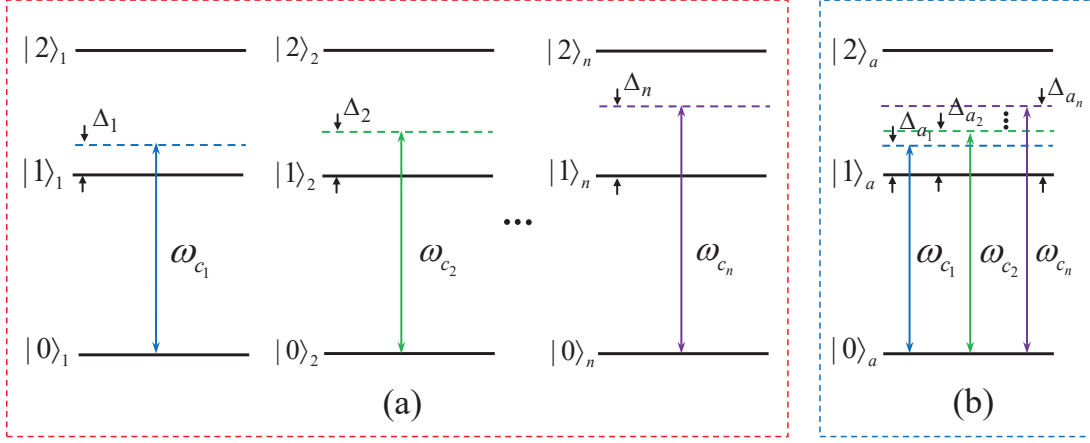


FIG. 6: (Color online) (a) Decoupling of qutrits $(1, 2, \dots, n)$ from their respective cavities before the gate operation (from left to right). Here, Δ_l is a large detuning between the frequency ω_{c_l} of cavity l and the $|0\rangle \leftrightarrow |1\rangle$ transition frequency of qutrit l ($l = 1, 2, \dots, n$), representing that cavity l is far-off resonant with (decoupled from) the $|0\rangle \leftrightarrow |1\rangle$ transition of qutrit l . (b) Decoupling of qutrit a from all n cavities before the gate operation. Here, Δ_{a_l} is a large detuning between the frequency ω_{c_l} of cavity l and the $|0\rangle \leftrightarrow |1\rangle$ transition frequency of qutrit a ($l = 1, 2, \dots, n$), indicating that cavity l is far-off resonant with (decoupled from) the $|0\rangle \leftrightarrow |1\rangle$ transition of qutrit a . During the gate operation, one needs to bring the $|0\rangle \leftrightarrow |1\rangle$ transition of qutrit a on resonance with cavity l , which can be met by setting $\Delta_{a_l} = 0$ ($l = 1, 2, \dots, n$). In addition, one needs to bring the $|0\rangle \leftrightarrow |1\rangle$ transition of qutrits l and a on resonance with cavity l , corresponding to $\Delta_l = \Delta_{a_l} = 0$ ($l = 1, 2, \dots, n$).

(i) U_1 transforms the state $|1\rangle$ of qutrit l to $|2\rangle$ ($l = 2, 3, \dots, n$). This transformation can be obtained by: Apply a classical pulse to each of qutrits $(2, 3, \dots, n)$, which is resonant with the $|1\rangle \leftrightarrow |2\rangle$ transition of the qutrits. Each pulse has an initial phase $-\pi/2$. The duration of the pulse applied to qutrit l is $\pi/(2\Omega_l)$.

(ii) U_2 leads to the state transform $|1\rangle_1 |0\rangle_a |0\rangle_{c_1} \rightarrow -|0\rangle_1 |1\rangle_a |0\rangle_{c_1}$, which can be realized by: Bring the $|0\rangle \leftrightarrow |1\rangle$ transition of qutrits 1 and a to resonance with cavity 1 for an interaction time $\pi/(\sqrt{2}g_1)$.

(iii) U_{l+1} ($l = 2, 3, \dots, n-1$) results in the state transformation $|0\rangle_l |1\rangle_a |0\rangle_{c_l} \rightarrow -|1\rangle_l |0\rangle_a |0\rangle_{c_l}$ while nothing to the state $|1\rangle_a |0\rangle_{c_l}$. This can be achieved by: Bring the $|0\rangle \leftrightarrow |1\rangle$ transition of qutrits l and a to resonance with cavity l for an interaction time $\pi/(\sqrt{2}g_l)$, then turn off the interaction between qutrit l and cavity l but let qutrit a continue resonantly interacting with cavity l for an additional interaction time $2\pi/g_l - \pi/(\sqrt{2}g_l)$.

(iv) U_{n+1} leads to the state transformation $|0\rangle_n |1\rangle_a |0\rangle_{c_n} \rightarrow -|1\rangle_n |0\rangle_a |0\rangle_{c_n}$ and $|1\rangle_a |0\rangle_{c_n} \rightarrow -|1\rangle_a |0\rangle_{c_n}$. This state transformation can be realized by: Bring the $|0\rangle \leftrightarrow |1\rangle$ transition of qutrits n and a to resonance with cavity n for an interaction time $\pi/(\sqrt{2}g_n)$, then turn off the interaction between qutrit n and cavity n but let qutrit a continue resonantly interacting with cavity n for an additional interaction time $\pi/g_n - \pi/(\sqrt{2}g_n)$.

(v) U_{n+l+1} ($l = 1, 2, \dots, n-1$) leads to the state transformation $|1\rangle_{n-l+1} |0\rangle_a |0\rangle_{c_{n-l+1}} \rightarrow -|0\rangle_{n-l+1} |1\rangle_a |0\rangle_{c_{n-l+1}}$ while nothing to the state $|1\rangle_a |0\rangle_{c_{n-l+1}}$. This can be obtained by: Bring the $|0\rangle \leftrightarrow |1\rangle$ transition of qutrit a to resonance with cavity $n-l+1$ for an interaction time $2\pi/g_{n-l+1} - \pi/(\sqrt{2}g_{n-l+1})$, then let qutrit a continue resonantly interacting with cavity $n-l+1$ and bring the $|0\rangle \leftrightarrow |1\rangle$ transition of qutrit $n-l+1$ to resonance with cavity $n-l+1$ for an interaction time $\pi/(\sqrt{2}g_{n-l+1})$.

(vi) U_{2n+1} results in the state transformation $|0\rangle_1 |1\rangle_a |0\rangle_{c_1} \rightarrow -|1\rangle_1 |0\rangle_a |0\rangle_{c_1}$, which can be realized by: Bring the $|0\rangle \leftrightarrow |1\rangle$ transition of qutrits 1 and a to resonance with cavity 1 for an interaction time $\pi/(\sqrt{2}g_1)$.

(vii) U_{2n+2} transforms the state $|2\rangle$ of qutrit l ($l = 2, 3, \dots, n$) to $|1\rangle$. This state transformation can be implemented by: Apply a classical pulse to each of qutrits $(2, 3, \dots, n)$, which is resonant with the $|1\rangle \leftrightarrow |2\rangle$ transition of the qutrits. Each pulse has an initial phase $\pi/2$. The duration of the pulse applied to qutrit l is $\pi/(2\Omega_l)$.

One can check that after the above $2n+2$ basic unitary operations, the n -qubit controlled phase gate, described by Eq. (9), was implemented with $n-1$ control qubits (i.e., qubits 1, 2, ..., and $n-1$, respectively distributed in cavities 1, 2, ..., and $n-1$) and a target qubit (i.e. qubit n in cavity n).

Before ending this section, several points need to be addressed as follows:

(a). The qutrits, not involved in each step of operation, need to be decoupled from the cavities during the cavity-qutrit interaction. The cavities need to be not excited during the application of the pulse. In addition, the unwanted coupling of the levels $|0\rangle$, $|1\rangle$, and $|2\rangle$, induced by the cavity or the pulse, should be negligible for each qutrit. In

principle, these conditions can be satisfied by adjusting the level spacings of the qutrits [34-40]. For example, the level spacings of superconducting qutrits can be rapidly adjusted by varying external control parameters (e.g., the magnetic flux applied to a superconducting loop of phase, transmon, Xmon, or flux qutrits; see, e.g., [34-37]); the level spacings of NV centers can be readily adjusted by changing the external magnetic field applied along the crystalline axis of each NV center [38,39]; and the level spacings of atoms/quantum dots can be adjusted by changing the voltage on the electrodes around each atom/quantum dot [40].

(b). As shown above, the ancillary qubit does not need to interact all cavities simultaneously. Instead, the ancillary qubit is only required to resonantly interact with each cavity one by one, which corresponds to the case when the detunings Δ_{a_1} , Δ_{a_2} , ..., and Δ_{a_n} are set to be zero one by one [Fig. 6(b)]. Note that the detuning Δ_{a_l} ($l = 1, 2, \dots, n$) can be set zero, by adjusting the level spacings of the ancillary qubit or adjusting the frequency of cavity l such that the transition frequency between the two levels $|0\rangle$ and $|1\rangle$ is equal to the frequency of cavity l . In practice, setting Δ_{a_1} , Δ_{a_2} , ..., and Δ_{a_n} to be zero one by one becomes a challenge in experiments as the number of cavities increases. Note that frequencies of the microwave cavities or resonators can be quickly tuned in 1-3 ns [41,42].

(c). It is preferable to use single-mode cavities, which can be designed with appropriate choice of cavity parameters. However, using single-mode cavities is not necessary. Multi-mode cavities may be used because one can choose one mode to interact with the qutrits while have all other modes well decoupled from the three levels of the qutrits. This can be achieved by choosing qutrits with a proper level structure or designing the level structure of qutrits (e.g., solid-state qutrits) with a proper choice of device parameters. In addition, the method presented here is applicable to 1D, 2D, or 3D cavities or resonators as long as the conditions described above can be met.

(d). A multi-qubit controlled NOT (CNOT) gate, with multiple qubits simultaneously controlling a single target qubit, is often called as a Toffoli gate, for which the state $|0\rangle$ ($|1\rangle$) of the target qubit flips to $|1\rangle$ ($|0\rangle$) when all control qubits are in the state $|1\dots1\rangle$ but nothing happens to the state of the target qubit otherwise. As is well known, an n -qubit Toffoli gate can be constructed by using the n -qubit controlled phase gate (9) plus two single-qubit Hadamard gates, which are performed on the target qubit before and after the n -qubit controlled phase gate (9) respectively. Each of the single-qubit Hadamard transformations, $|0\rangle \rightarrow (|0\rangle + |1\rangle)/\sqrt{2}$ and $|1\rangle \rightarrow (|0\rangle - |1\rangle)/\sqrt{2}$, can be performed by applying a $\pi/2$ classical pulse resonant with the $|0\rangle \leftrightarrow |1\rangle$ transition of the target qubit. By combining with the above controlled-phase gate operations, one can implement an n -qubit Toffoli gate with only $2n + 4$ basic operations. Thus, the present method also provides a simple way to realize a multi-qubit Toffoli gate with qubits distributed in different cavities.

IV. DISCUSSION

In this section we discuss issues that are important to experimental implementation. For the method to work, the following requirements need to be satisfied. First, the total operation time

$$\tau = \pi/\Omega + \sqrt{2}\pi/g_1 + \sum_{j=3}^n 4\pi/g_{j-1} + 3\pi/g_n + (6n - 5)\tau_a \quad (11)$$

should be much shorter than the energy relaxation time T_1 and dephasing time T_2 of the level $|2\rangle$ of qutrits. Here, we have set $\Omega_l \equiv \Omega$ for simplicity, which can be achieved by adjusting the intensity of pulses applied to the qutrits, and τ_a is the typical time required for adjusting the level spacings of a single qutrit. Second, the lifetime of the mode of each cavity is given by $\kappa_l^{-1} = Q_l/\omega_{c_l}$ with Q_l being the quality factor of cavity l ($l = 1, 2, \dots, n$), which should be much longer than a single qutrit-cavity interaction time. Last, crosstalk between different cavities needs to be negligible since this interaction is not intended.

These requirements can in principle be realized, since (i) τ can be reduced by increasing the coupling constant g_l ($l = 1, 2, \dots, n$) (i.e., each qutrit is placed at an antinode of the cavity mode), (ii) τ_a can be shortened by rapid adjustment of the level spacings of the qutrits (e.g., the typical time is 1 - 3 ns for adjusting the level spacings of a superconducting qutrit [35,43,44]), (iii) κ_l^{-1} can be increased by employing a high- Q_l cavity so that the cavity dissipation is negligible during the operation, (iv) the qutrits can be chosen or designed so that the energy relaxation time T_1 and the dephasing time T_2 of the level $|2\rangle$ are sufficiently long, and (v) direct crosstalk between cavities can be made negligibly small as long as $\Delta_{kl} \gg g_{kl}$. Here, Δ_{kl} is the frequency difference between cavities k and l , g_{kl} is the coupling strength between cavities k and l , with $k, l \in \{1, 2, \dots, n\}$ and $k \neq l$.

V. POSSIBLE EXPERIMENTAL IMPLEMENTATION IN CIRCUIT QED

Circuit QED, consisting of microwave cavities and superconducting qubits, is particularly attractive and considered as one of the leading candidates for QIP [45-52]. In the past decade, based on circuit QED, much progress has been made in quantum state preparation, quantum logic gate implementation, quantum state transfer, etc. with superconducting qubits or microwave photons (see the review articles [49-52]). For the sake of definitiveness, let us

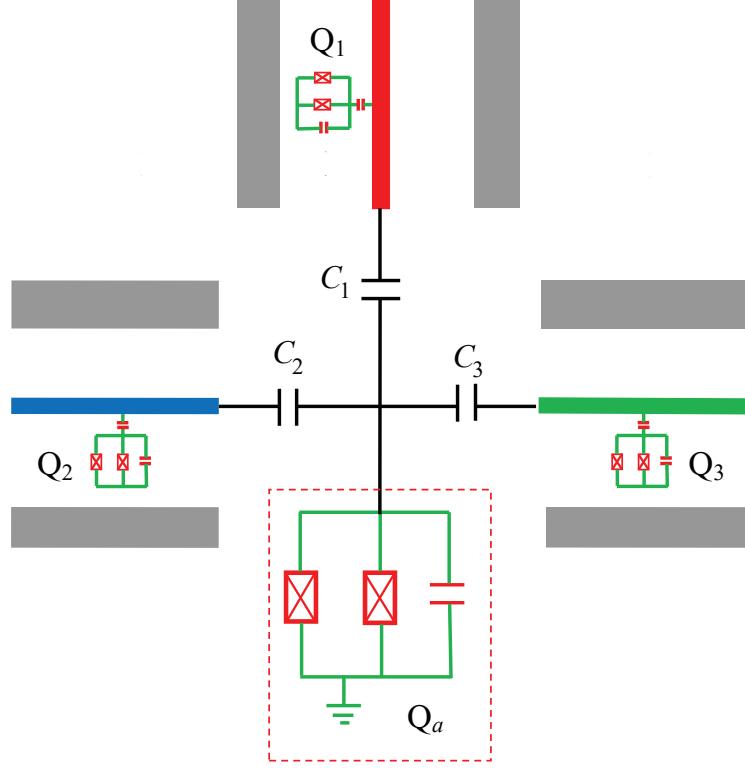


FIG. 7: (Color online) Setup for three cavities each hosting a superconducting transmon qutrit and coupled by an ancillary transmon qutrit. Each cavity here is a one-dimensional coplanar resonator, consisting of a central waveguide line and two lateral ground planes. Q_1 , Q_2 , and Q_3 represent three transmon qutrits 1, 2, and 3, which are capacitively coupled to their respective cavities. Q_a represents the coupler qutrit a , which is capacitively coupled to the three cavities via capacitance C_1 , C_2 , and C_3 , respectively. The electronic circuit of a transmon qutrit consists of two Josephson junctions and a capacitor.

now consider the experimental feasibility of realizing a three-qubit controlled phase gate, which act on three qubits distributed in three different cavities. The three-qubit gate here is implemented by using a circuit QED system, which consists of three identical superconducting transmon qutrits (1, 2, 3) respectively embedded in three cavities (1, 2, 3), which are coupled to an auxiliary transmon qutrit a (Fig. 7). Note that the three qubits (1,2,3) involved in the gate correspond to the three transmon qutrits (1,2,3), respectively. For a transmon qutrit, its design is closely related to the Cooper pair box (CPB) with two Josephson junctions [63]. Thus, it is noted that the coupling mechanism of a transmon qutrit and a cavity is the same as that of a CPB and a cavity.

Each cavity considered in Fig.7 is a one-dimensional coplanar resonator (TLR), which consists of a central waveguide line and two lateral ground planes. After quantization of the cavity field, there is a standing-wave distribution of quantum voltage along the central waveguide line of the cavity. The quantum voltage is caused by the electric field of the cavity mode. As shown in Fig. 7, the transmon qutrit hosted in each cavity is capacitively coupled to the cavity, by a capacitor connecting to the central waveguide line of the TLR and the transmon qutrit [37,63,53-55]. This capacitive coupling is induced due to the quantum voltage exerted on the coupling capacitor [63] (also, see [4,47]). Alternatively, the transmon qutrit hosted in each cavity can be coupled to the cavity by the cavity magnetic field threading the superconducting loop of the qutrit [56-58]. The qutrit-cavity coupling strength can be varied by adjusting the loop size of the qutrit, the position of the qutrit in the cavity, or the coupling capacitance.

In Fig. 7, the coupling mechanism for the ancillary transmon qutrit capacitively coupled to each cavity is the same as that for the intra-cavity transmon qutrit capacitively coupled to the corresponding cavity. To have the ancillary transmon qutrit coupled to cavity l ($l = 1, 2, 3$), the quantum voltage at one end of the central guide line of cavity l , which connects the coupling capacitor C_l , should be not zero. This requirement can be met by a prior design of cavity, such that that end of the central waveguide line is an antinode of the quantum voltage. It is noted that the coupling strength of the ancillary transmon qutrit with each cavity can be varied by a prior design of the sample with an appropriate coupling capacitance.

From the description given in Sec. III, the gate implementation involves the following three basic operations:

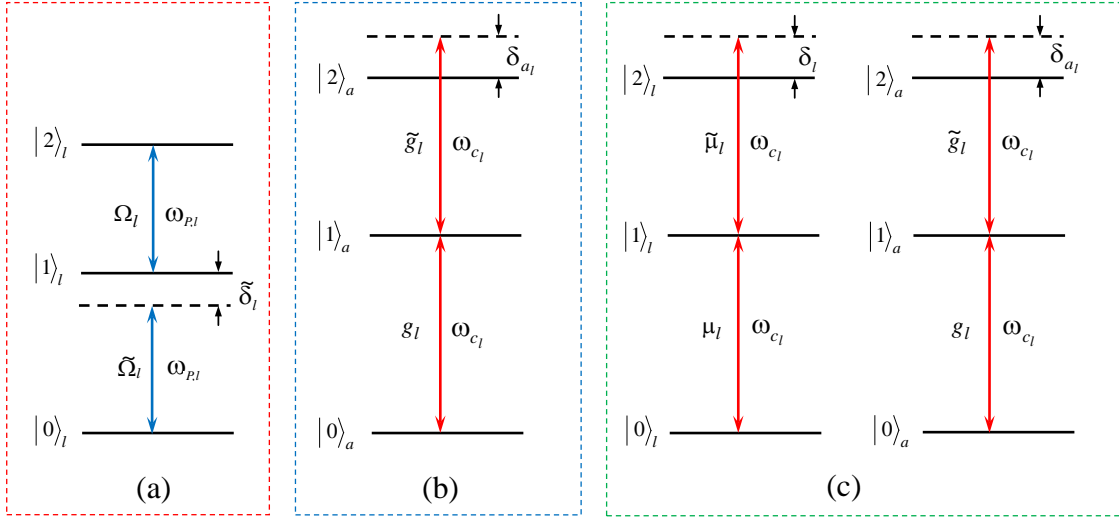


FIG. 8: (Color online) (a) A classical pulse is resonant with the $|1\rangle \leftrightarrow |2\rangle$ transition of qutrit l with a Rabi frequency Ω_l , while off-resonant with the $|0\rangle \leftrightarrow |1\rangle$ transition of qutrit l with a Rabi frequency $\tilde{\Omega}_l$ and detuning $\tilde{\delta}_l$ ($l = 1, 2, 3$). (b) Cavity l is resonant with the $|0\rangle \leftrightarrow |1\rangle$ transition of qutrit a with a coupling constant g_l , while off-resonant with the $|1\rangle \leftrightarrow |2\rangle$ transition of qutrit a with a coupling constant \tilde{g}_l and detuning δ_{a_l} ($l = 1, 2, 3$). (c) Cavity l is simultaneously resonant with the $|0\rangle \leftrightarrow |1\rangle$ transition of qutrits l and a , with a coupling constant μ_l for qutrit l and a coupling constant g_l for qutrit a ($l = 1, 2, 3$). In addition, cavity l is off-resonant with the $|1\rangle \leftrightarrow |2\rangle$ transition of qutrits l and a , with a coupling constant $\tilde{\mu}_l$ and detuning δ_l for qutrit l , while a coupling constant \tilde{g}_l and detuning δ_{a_l} for qutrit a ($l = 1, 2, 3$). For the definition of the detunings $\tilde{\delta}_l$, δ_l , and δ_{a_l} , refer to the text.

(i) The first basic operation is described by the Hamiltonian H_{I_1} in Eq. (1). In reality, the inter-cavity crosstalk between the two cavities is inevitable [59], and there exists the unwanted coupling of the pulse with the $|0\rangle \leftrightarrow |1\rangle$ transition. When these factors are taken into account, the Hamiltonian H_{I_1} is modified as

$$\tilde{H}_{I_1} = \hbar (\Omega_l e^{i\phi_l} |1\rangle_l \langle 2| + \text{h.c.}) + \hbar (\tilde{\Omega}_l e^{i\phi_l} e^{-i\tilde{\delta}_l t} |0\rangle_l \langle 1| + \text{h.c.}) + \varepsilon, \quad (12)$$

where the first bracket term represents the resonant interaction of the pulse with the $|1\rangle \leftrightarrow |2\rangle$ transition of qutrit l ($l = 2, 3$), while the second bracket term represents the unwanted interaction of the pulse with the $|0\rangle \leftrightarrow |1\rangle$ transition with Rabi frequency $\tilde{\Omega}_l$ and detuning $\tilde{\delta}_l = \tilde{\omega}_{10,l} - \omega_{p,l} > 0$ ($\omega_{p,l}$ is the frequency of the pulse applied to qutrit l) [Fig. 8(a)]. Note that the transition frequencies of qutrit l when interacting with a classical pulse are different from those of qutrit l when interacting with cavity l . Thus, we here define $\tilde{\omega}_{10,l}$ ($\tilde{\omega}_{21,l}$) as the $|0\rangle \leftrightarrow |1\rangle$ ($|1\rangle \leftrightarrow |2\rangle$) transition frequency of qutrit l when interacting with a pulse, but we will later use different notations to define the transition frequencies of qutrit l when interacting with cavity l . The detuning $\tilde{\delta}_l$ can be further written as $\tilde{\delta}_l = \tilde{\omega}_{10,l} - \tilde{\omega}_{21,l} = \delta\tilde{\omega}_l$ because of $\omega_{p,l} = \tilde{\omega}_{21,l}$. Here, $\delta\tilde{\omega}_l$ is the anharmonicity between the $|0\rangle \leftrightarrow |1\rangle$ level spacing and the $|1\rangle \leftrightarrow |2\rangle$ level spacing of qutrit l . The last term ε in Eq. (11) represents the inter-cavity crosstalk of cavities, which is given by

$$\varepsilon = g_{12} (e^{i\Delta_{12}t} a_1 a_2^\dagger + \text{h.c.}) + g_{23} (e^{i\Delta_{23}t} a_2 a_3^\dagger + \text{h.c.}) + g_{13} (e^{i\Delta_{13}t} a_1 a_3^\dagger + \text{h.c.}), \quad (13)$$

where g_{12} , g_{23} , and g_{13} are the coupling strengths of cavities (1,2), (2,3), and (1,3), respectively; while $\Delta_{12} = \omega_{c_2} - \omega_{c_1}$, $\Delta_{23} = \omega_{c_3} - \omega_{c_2}$, and $\Delta_{13} = \omega_{c_3} - \omega_{c_1}$ are the cavity-frequency detunings.

(ii) The second basic operation is described by the Hamiltonian H_{I_2} in Eq. (3). In practice, the inter-cavity crosstalk between the three cavities and the unwanted coupling of cavity l ($l = 1, 2, 3$) with the $|1\rangle \leftrightarrow |2\rangle$ transition of qutrit a should be considered. When these factors are taken into account, the Hamiltonian H_{I_2} is modified as

$$\tilde{H}_{I_2} = \hbar (g_l a_l^\dagger |0\rangle_a \langle 1| + \text{h.c.}) + \hbar (\tilde{g}_l e^{i\delta_{a_l} t} a_l^\dagger |1\rangle_a \langle 2| + \text{h.c.}) + \varepsilon, \quad (14)$$

where the first bracket term represents the resonant interaction of cavity l with the $|0\rangle \leftrightarrow |1\rangle$ transition of qutrit a , while the second bracket term represents the unwanted coupling between cavity l and the $|1\rangle \leftrightarrow |2\rangle$ transition of

qutrit a with coupling strength \tilde{g}_l and detuning $\delta_{a_l} = \omega_{c_l} - \omega_{21,l}^a > 0$ [Fig. 8(b)]. Here and below, we define $\omega_{21,l}^a$ ($\omega_{10,l}^a$) as the $|1\rangle \leftrightarrow |2\rangle$ ($|0\rangle \leftrightarrow |1\rangle$) transition frequency of qutrit a in the case when qutrit a interacts with cavity l . Note that both of $\omega_{21,l}^a$ and $\omega_{10,l}^a$ change with the index l (i.e., the qutrit-cavity interaction switches from one cavity to another). The detuning δ_{a_l} can also be written as $\delta_{a_l} = \omega_{10,l}^a - \omega_{21,l}^a = \delta\omega_l^a$ because of $\omega_{c_l} = \omega_{10,l}^a$. Here, $\delta\omega_l^a$ is the anharmonicity between the $|0\rangle \leftrightarrow |1\rangle$ level spacing and the $|1\rangle \leftrightarrow |2\rangle$ level spacing of qutrit a . The last term of Eq. (17) represents the inter-resonator crosstalk, which is described by Eq. (12) given above.

(iii) The third basic operation is described by the Hamiltonian H_{I_3} in Eq. (5). In reality, the inter-cavity crosstalk between the three cavities and the unwanted coupling of cavity l ($l = 1, 2, 3$) with the $|1\rangle \leftrightarrow |2\rangle$ transition of both qutrit a and qutrit l need to be considered. After taking these factors into account, the Hamiltonian H_{I_3} becomes

$$\begin{aligned} \tilde{H}_{I_3} = & \hbar(\mu_l a_l^\dagger |0\rangle_l \langle 1| + \text{h.c.}) + \hbar(g_l a_l^\dagger |0\rangle_a \langle 1| + \text{h.c.}) \\ & + \hbar(\tilde{\mu}_l e^{i\delta_l t} a_l^\dagger |0\rangle_l \langle 1| + \text{h.c.}) \\ & + \hbar(\tilde{g}_l e^{i\delta_{a_l} t} a_l^\dagger |0\rangle_a \langle 1| + \text{h.c.}) \\ & + \varepsilon, \end{aligned} \quad (15)$$

where the first (second) bracket term in the first line represent the resonant interaction of cavity l with the $|0\rangle \leftrightarrow |1\rangle$ transition of qutrit l (a), the term in the second line represent the unwanted coupling between cavity l and the $|1\rangle \leftrightarrow |2\rangle$ transition of qutrit l with coupling strength \tilde{g}_l and detuning $\delta_l = \omega_{c_l} - \omega_{21,l} = \omega_{10,l} - \omega_{21,l} = \delta\omega_l > 0$ [Fig. 8(c)], while the term in the third line represent the unwanted coupling between cavity l and the $|1\rangle \leftrightarrow |2\rangle$ transition of qutrit a with coupling strength \tilde{g}_l and detuning δ_{a_l} described above. Here, $\omega_{10,l}$ ($\omega_{21,l}$) represents the $|0\rangle \leftrightarrow |1\rangle$ ($|1\rangle \leftrightarrow |2\rangle$) transition frequency of qutrit l . We have applied $\omega_{c_l} = \omega_{10,l}$ in writing $\delta_l = \delta\omega_l$. Here, $\delta\omega_l$ is the anharmonicity between the $|0\rangle \leftrightarrow |1\rangle$ level spacing and the $|1\rangle \leftrightarrow |2\rangle$ level spacing of qutrit l .

By considering dissipation and dephasing, the evolution of the system is determined by the master equation

$$\begin{aligned} \frac{d\rho}{dt} = & -i \left[\tilde{H}_{I_k}, \rho \right] + \sum_{l=1}^3 \kappa_{a_l} \mathcal{L}[a_l] \\ & + \sum_{l=1,2,3,a} \gamma_{12,l} \mathcal{L}[\sigma_{12,l}^-] + \gamma_{02,l} \mathcal{L}[\sigma_{02,l}^-] + \gamma_{01,l} \mathcal{L}[\sigma_{01,l}^-] \\ & + \sum_{l=1,2,3,a} \gamma_{2\varphi,l} (\sigma_{22,l} \rho \sigma_{22,l} - \sigma_{22,l} \rho / 2 - \rho \sigma_{22,l} / 2) \\ & + \sum_{l=1,2,3,a} \gamma_{1\varphi,l} (\sigma_{11,l} \rho \sigma_{11,l} - \sigma_{11,l} \rho / 2 - \rho \sigma_{11,l} / 2), \end{aligned} \quad (16)$$

where \tilde{H}_{I_k} (with $k = 1, 2, 3$) are the modified Hamiltonians \tilde{H}_{I_1} , \tilde{H}_{I_2} , and \tilde{H}_{I_3} , $\mathcal{L}[\Lambda] = \Lambda \rho \Lambda^\dagger - \Lambda^\dagger \Lambda \rho / 2 - \rho \Lambda^\dagger \Lambda / 2$ (with $\Lambda = a_l, \sigma_{12,l}^-, \sigma_{02,l}^-, \sigma_{01,l}^-$), $\sigma_{12,l}^- = |1\rangle_l \langle 2|$, $\sigma_{02,l}^- = |0\rangle_l \langle 2|$, $\sigma_{01,l}^- = |0\rangle_l \langle 1|$, $\sigma_{22,l} = |2\rangle_l \langle 2|$, and $\sigma_{11,l} = |1\rangle_l \langle 1|$; κ_{a_l} is the decay rate of cavity l ($l = 1, 2, 3$); $\gamma_{12,l}$ ($\gamma_{02,l}$) is the energy relaxation rate for the level $|2\rangle$ associated with the decay path $|2\rangle \rightarrow |1\rangle$ ($|2\rangle \rightarrow |0\rangle$) of qutrit l ; $\gamma_{01,l}$ is the energy relaxation rate of the level $|1\rangle$; and $\gamma_{2\varphi,l}$ ($\gamma_{1\varphi,l}$) is the dephasing rate of the level $|2\rangle$ ($|1\rangle$) of qutrit l ($l = 1, 2, 3, a$).

The fidelity of the whole operation is given by $\mathcal{F} = \sqrt{\langle \psi_{\text{id}} | \rho | \psi_{\text{id}} \rangle}$, where $|\psi_{\text{id}}\rangle$ is the ideal output state obtained under the theoretical model, while ρ is the final density matrix obtained by numerically solving the master equation. As an example, we consider an input state of the whole system $\frac{1}{2\sqrt{2}} \sum |i_1 i_2 i_3\rangle \otimes |0\rangle_a |0\rangle_c$, with $i_1, i_2, i_3 \in \{0, 1\}$. Thus, the ideal output state is $|\psi_{\text{id}}\rangle = \frac{1}{2\sqrt{2}} \left(\sum_{i_1, i_2, i_3 \neq 1} |i_1 i_2 i_3\rangle - |111\rangle \right) \otimes |0\rangle_a |0\rangle_c$.

We now numerically calculate the fidelity. The anharmonicity of the level spacings for a transmon qutrit can be made to be within 100 ~ 600 MHz [60]. Note that the anharmonicity of the level spacings of a transmon qutrit slightly varies during adjusting the qutrit level spacings. Thus, we can choose $\delta\omega_l/2\pi \sim \delta\omega_{a_l}/2\pi \sim \delta\tilde{\omega}_l/2\pi = 600$ MHz ($l = 1, 2, 3$). For a TLR, the typical frequency is 1 – 10 GHz. Therefore, we choose $\omega_{c_1}/2\pi = 5.0$ GHz, $\omega_{c_2}/2\pi = 6.0$ GHz, and $\omega_{c_3}/2\pi = 7.0$ GHz, resulting in $\Delta_{12}/2\pi = \Delta_{23}/2\pi = 1$ GHz and $\Delta_{23}/2\pi = 2$ GHz. We choose $\mu_l/2\pi = g_l/2\pi = g/2\pi = 10$ MHz and $\Omega_l/2\pi = \Omega/2\pi = 15$ MHz ($l = 1, 2, 3$), which are available in experiments [61,62]. For a transmon qutrit [63], one has $\tilde{\mu}_l \sim \sqrt{2}\mu_l$, $\tilde{g}_l \sim \sqrt{2}g_l$, and $\tilde{\Omega}_l \sim \Omega/\sqrt{2}$. Other parameters used in the numerical simulations are: (i) $\gamma_{1\varphi,l}^{-1} = 15$ μs , $\gamma_{2\varphi,l}^{-1} = 15$ μs ; (ii) $\gamma_{01,l}^{-1} = 20$ μs , $\gamma_{12,l}^{-1} = 10$ μs , $\gamma_{02,l}^{-1} = 25$ μs ($l = 1, 2, 3, a$), and (iii) $\kappa_{a_l}^{-1} = 10$ μs ($l = 1, 2, 3$). It should be mentioned that the decoherence times chosen here is a conservative case because the energy relaxation time and the dephasing time can be made to be on the order of

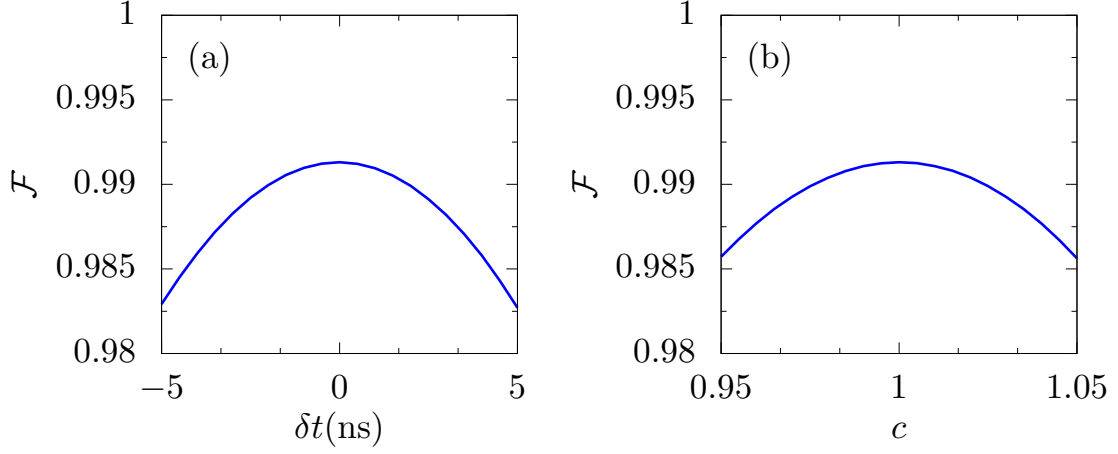


FIG. 9: (Color online) (a) Fidelity versus δt . Here, δt is an error, which applies to each typical interaction time. (b) Fidelity versus $c = \mu_l/g_l$. For the definition of μ_l and g_l , see the text.

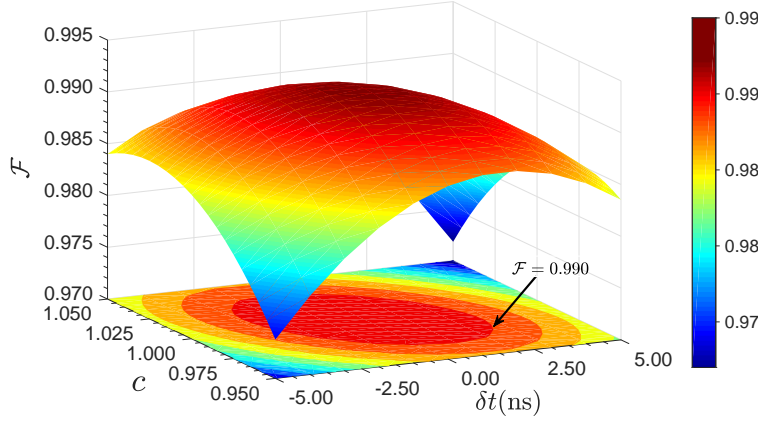


FIG. 10: (Color online) (a) Fidelity versus δt and c . Here, δt is an error for each typical interaction time. In addition, $c = \mu_l/g_l$.

25 – 100 μs for the state-of-the-art superconducting transmon devices at the present time [64-67]. For simplicity, we choose $g_{12} = g_{23} = g_{13} = 0.1g$ in our numerical simulations.

To investigate the effect of the operation time error on the fidelity, we apply an error δt to each interaction time as described in the previous section. With this modification, we numerically calculate the fidelity and plot Fig. 9(a). Figure 9(a) shows that the fidelity is sensitive to the operation time error but a high fidelity greater than 98.8% can be reached for $\delta t \in [-5, 5]$ ns, i.e., corresponding to a 10% error in each typical operation time, which is ~ 50 ns based on the values of g and Ω chosen above.

In a realistic situation, it may be a challenge to meet the condition $\mu_l = g_l$ ($l = 1, 2, 3$). Thus, we consider a small difference between μ_l and g_l . We set $\mu_l = cg_l$ with $c \in [0.95, 1.05]$. Here, $g_l/2\pi = g/2\pi = 10$ MHz. We numerically calculate the fidelity and plot Fig. 9(b). Figure 9(b) demonstrates that for $c \in [0.95, 1.05]$, the fidelity is greater than 99.1%.

We further plot Fig. 10, which shows the fidelity versus the operation time error δt and the coupling-strength ratio $c = \mu_l/g_l$. From Fig. 10, one can see that the fidelity can reach 0.99 or greater for $-3 \text{ ns} \leq \delta t \leq 3 \text{ ns}$ and $0.97 \leq c \leq 1.03$, i.e., the area indicated by the red circle at the bottom of Fig. 10.

The entire operation time is $\sim 0.5 \mu\text{s}$ for the values of g and Ω given above. Note that the operation time can be shortened by increasing g and Ω . For instance, the entire operation time could be ~ 50 ns if we choose $g/2\pi = 100$ MHz and $\Omega/2\pi = 150$ MHz. However, due to the smaller anharmonicity of the level spacings for a transmon qutrit, increasing g and Ω may decrease the fidelity, because the effect of the unwanted $|0\rangle \leftrightarrow |1\rangle$ coupling (induced by the

pulse) and the effect of the unwanted $|1\rangle \leftrightarrow |2\rangle$ coupling (caused by the cavity mode) become more apparent as g and Ω increase.

As discussed in [68,69], as long as the cavities are physically well separated, the inter-cavity crosstalk coupling strength is $g_{lk} \approx g_l (C_l/C_\Sigma)$ ($lk = 12, 23, 13$), where $C_\Sigma = C_1 + C_2 + C_3 + C_a$ is the sum of the three coupling capacitances and the qutrit a 's capacitance. For $C_1, C_2, C_3 \sim 1$ fF and $C_\Sigma \sim 10^2$ fF (the typical values in experiments [68,69]), we have $g_{lk} \leq 0.1g_l$. Note that in the numerical simulations, we set $g_l = g$. Thus, the condition $g_{lk} = 0.1g$ ($lk = 12, 23, 13$) can be easily satisfied.

For the cavity frequencies given above and $\kappa_{a_l}^{-1} = 10 \mu\text{s}$, the required quality factors for the three cavities are $Q_1 = 3.1 \times 10^5$, $Q_2 = 3.8 \times 10^5$, and $Q_3 = 4.4 \times 10^5$. The required cavity quality factors here are achievable in experiments because TLRs with a (loaded) quality factor $Q \sim 10^6$ have been experimentally demonstrated [70,71]. Our analysis here implies that high-fidelity implementation of a three-qubit controlled phase gate, which act on three qubits distributed in three different cavities, is feasible with present circuit QED technology.

It is worth noting that the capacitive coupling of a superconducting transmon qutrit to two one-dimension transmission line resonators has been experimentally implemented [72]. With rapid development of the circuit QED technology, we think that the setup illustrated in Fig. 7, which consists of three one-dimension transmission line resonators capacitively coupled to a single transmon qutrit, will soon be realized in experiments.

VI. THREE-QUBIT CONTROLLED PHASE GATE WITH ATOMS USING A SINGLE CAVITY

The above method can be generalized to implement an n -qubit controlled phase gate with $n + 1$ atoms, by using one cavity. To see this, let us consider a three-qubit case. We will give a detailed discussion on realizing a three-qubit controlled phase gate described above, using atoms interacting with a single cavity.

Consider four identical three-level atoms ($1, 2, 3, a$) and a single cavity. Each atom has three levels as shown in Fig. 2(b). Suppose that the transition between the two levels $|0\rangle$ and $|1\rangle$ of each atom is resonantly coupled to the cavity with a coupling constant g , while the transition between any other two levels is highly detuned or decoupled from the cavity mode. In addition, assume that the cavity is initially in the vacuum state. Each atom is trapped in the periodic potential of a one-dimensional optical lattice and can be loaded into or moved out of the cavity by translating the optical lattice [73]. Alternatively, each atom is trapped in an optical dipole trap and can be loaded into or moved out of the cavity by translating the optical dipole trap [74].

According to the gate operations described in subsection III A, one can easily find that the procedure for implementing the three-qubit controlled phase gate is listed below:

Step 1: Apply a classical pulse to each of atoms ($2, 3$), which has an initial phase $-\pi/2$ and is resonant with the $|1\rangle \leftrightarrow |2\rangle$ transition [Fig. 11(a)]. The Rabi frequency of the pulse applied to atom l is Ω ($l = 2, 3$). After an interaction time $\tau_1 = \pi/(2\Omega)$, the state $|1\rangle$ of atom l changes to $|2\rangle$ according to Eq. (2).

Step 2: Move atoms 1 and a to resonance with cavity 1 for an interaction time $\tau_2 = \pi/(\sqrt{2}g)$ [Fig. 11(b)], resulting in the state transformation $|1\rangle_1 |0\rangle_a |0\rangle_{c_1} \rightarrow -|0\rangle_1 |1\rangle_a |0\rangle_{c_1}$ according to Eq. (6).

Step 3: Move atom 1 out of the cavity but move atom 2 into the cavity and keep atom a in the cavity to have atoms 2 and a to resonance with cavity 2 for an interaction time $\tau_{3,1} = \pi/(\sqrt{2}g)$ [Fig. 11(c)], resulting in $|0\rangle_2 |1\rangle_a |0\rangle_{c_3} \rightarrow -|1\rangle_2 |0\rangle_a |0\rangle_{c_2}$ according to Eq. (6). Then move atom 2 out of the cavity such that the state $-|1\rangle_2 |0\rangle_a |0\rangle_{c_2}$ remains unchanged, while let atom a continue resonantly interacting with cavity 2 for an additional interaction time $\tau_{3,2} = 2\pi/g - \pi/(\sqrt{2}g)$ [Fig. 11(d)]. After an interaction time $\tau_3 = \tau_{3,1} + \tau_{3,2} = 2\pi/g$, the state $|1\rangle_a |0\rangle_{c_2}$ remains unchanged according to Eq. (4).

Step 4: Move atom 3 into the cavity and keep atom a in the cavity to have atoms 3 and a to resonance with cavity 3 for an interaction time $\tau_{4,1} = \pi/(\sqrt{2}g)$ [Fig. 11(e)], resulting in $|0\rangle_3 |1\rangle_a |0\rangle_{c_3} \rightarrow -|1\rangle_3 |0\rangle_a |0\rangle_{c_3}$ according to Eq. (6). Then, move atom 3 out of the cavity such that the state $-|1\rangle_3 |0\rangle_a |0\rangle_{c_3}$ remains unchanged, while let atom a continue resonantly interacting with cavity 3 for an additional interaction time $\tau_{4,2} = \pi/g - \pi/(\sqrt{2}g)$ [Fig. 11(d)]. After an interaction time $\tau_4 = \tau_{4,1} + \tau_{4,2} = \pi/g$, the state $|1\rangle_a |0\rangle_{c_3}$ becomes $-|1\rangle_a |0\rangle_{c_3}$ according to Eq. (4).

Step 5: Let atom a to resonance with cavity 3 for an interaction time $\tau_{5,1} = 2\pi/g - \pi/(\sqrt{2}g)$ [Fig. 11(d)]. Then, keep atom a in the cavity and move atom 3 into the cavity to have atoms a and 3 to resonance with cavity 3 for an interaction time $\tau_{5,2} = \pi/(\sqrt{2}g)$ [Fig. 11(e)]. After the interaction time $\tau_{5,2}$, we have the state transformation $|1\rangle_3 |0\rangle_a |0\rangle_{c_3} \rightarrow -|0\rangle_3 |1\rangle_a |0\rangle_{c_3}$ according to Eq. (6), while after an interaction time $\tau_5 = \tau_{5,1} + \tau_{5,2} = 2\pi/g$ the state $|1\rangle_a |0\rangle_{c_3}$ remains unchanged according to Eq. (4).

Step 6: Move atom 3 out of the cavity but let atom a to resonance with the cavity for an interaction time $\tau_{6,1} = 2\pi/g - \pi/(\sqrt{2}g)$ [Fig. 11(d)]. Then, move atom 2 into the cavity and keep atom a in the cavity to have atoms 2 and a to resonantly interact with the cavity for an interaction time $\tau_{6,2} = \pi/(\sqrt{2}g)$ [Fig. 11(c)]. After the interaction time $\tau_{6,2}$, one has the state transformation $|1\rangle_2 |0\rangle_a |0\rangle_{c_2} \rightarrow -|0\rangle_2 |1\rangle_a |0\rangle_{c_2}$ according to Eq. (6), while after an interaction time $\tau_6 = \tau_{6,1} + \tau_{6,2} = 2\pi/g$ the state $|1\rangle_a |0\rangle_{c_2}$ remains unchanged according to Eq. (4).

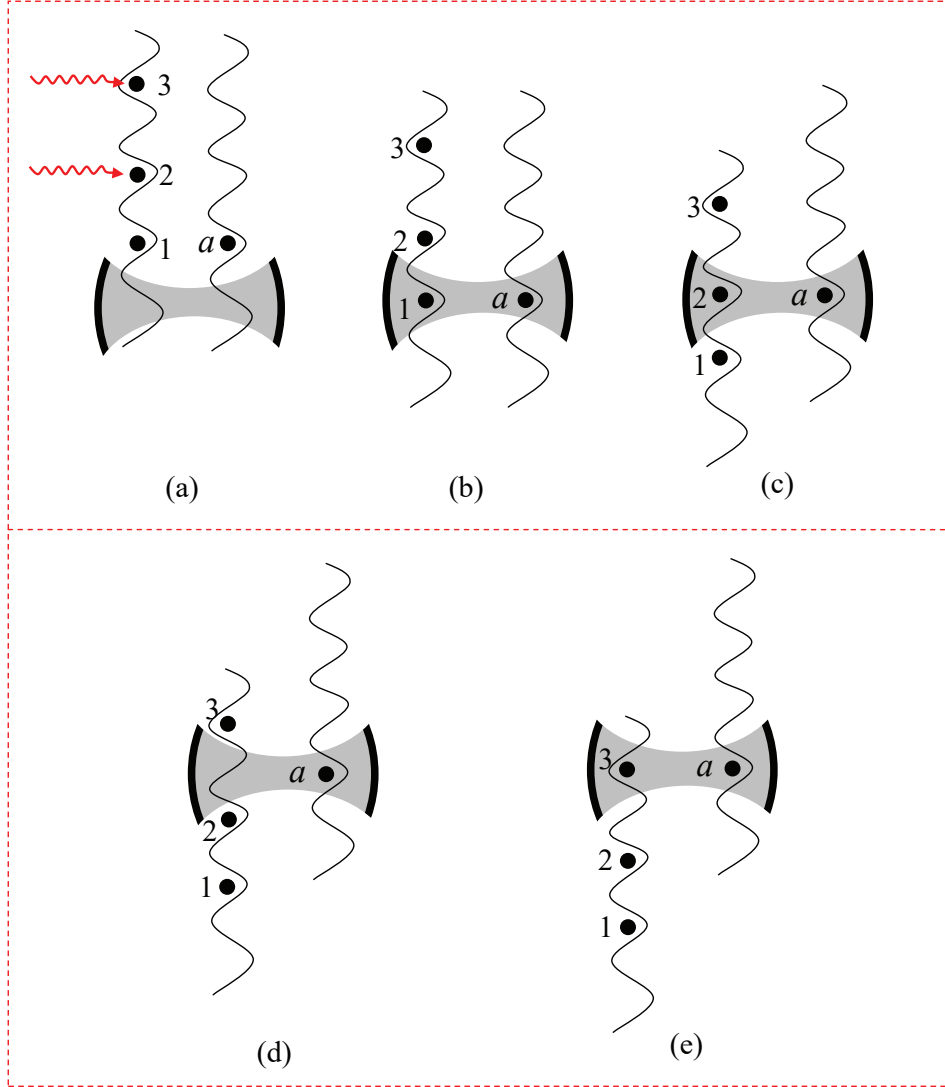


FIG. 11: (Color online) Proposed setup for a three-qubit controlled phase gate with four identical neutral atoms (1, 2, 3, a) and a cavity. Each atom can be either loaded into the cavity or moved out of the cavity by one-dimensional translating optical lattices [73] or an optical dipole trap [74]. Atoms 1 and 2 play a role of controlled qubits while atom 3 acts as a target qubit. In addition, atom a is an auxiliary system, which is used for the coherent manipulation.

Step 7: Move atom 2 out of the cavity but move atom 1 into the cavity to have atoms 1 and a to resonance with the cavity for an interaction time $\tau_7 = \pi/(\sqrt{2}g)$ [Fig. 11(b)], resulting in the state transformation $|0\rangle_1 |1\rangle_a |0\rangle_{c_1} \rightarrow -|1\rangle_1 |0\rangle_a |0\rangle_{c_1}$ according to Eq. (6).

Step 8: Move atoms 1 and a out of the cavity [Fig. 11(a)]. Then, apply a classical pulse to each of atoms (2, 3), which has an initial phase $\pi/2$ and is resonant with the $|1\rangle \leftrightarrow |2\rangle$ transition of the atoms. The Rabi frequency of the pulse applied to atom l is Ω ($l = 2, 3$). After a pulse duration $\tau_8 = \pi/(2\Omega)$, the state $|2\rangle$ of atom l changes to $|1\rangle$ according to Eq. (2).

The total operation time is $\tau = \pi/\Omega + (\sqrt{2} + 7)\pi/g + 10\tau_m$. Here, τ_m is the typical time required for moving atoms into or out of the cavity. For the proposal to work, the τ should be much smaller than the energy relaxation time of

level $|1\rangle$ or $|2\rangle$, such that the decoherence induced due to the spontaneous decay of the level $|1\rangle$ or $|2\rangle$ is negligible. In addition, it is noted that during the gate operation, the longest single atom-cavity interaction time is $2\pi/g$, which should be much shorter than the cavity decay time κ^{-1} , so that the cavity dissipation is negligible. In principle, these conditions can be satisfied by choosing a cavity with a high quality factor Q and atoms with a sufficiently long energy relaxation time.

To investigate the experimental feasibility of this proposal, let us consider Rydberg atoms with principal quantum numbers 49–51 (respectively corresponding to the levels $|0\rangle$, $|1\rangle$, and $|2\rangle$). The $|0\rangle \leftrightarrow |1\rangle$ transition frequency is $\omega_0/2\pi \sim 51.1$ GHz, the energy relaxation time T_{rad} of the level $|1\rangle$ or $|2\rangle$ is on the order of 10^{-2} s [75], and the coupling constant is $g = 2\pi \times 50$ KHz [75,76]. In addition, choose $\Omega = 2\pi \times 50$ KHz. With the choice of these parameters, the time needed for the entire operation is $\tau \sim 104 \mu\text{s}$ for $\tau_{\text{m}} \sim 1 \mu\text{s}$ [4], which is much shorter than T_{rad} by two orders of magnitude. The cavity mode frequency is $\omega_c/2\pi \sim 51.1$ GHz, thus the lifetime of the cavity photon is $T_c = Q/\omega_c \sim 200 \mu\text{s}$ for a cavity with $Q = 6.4 \times 10^7$, which is much larger than the longest single atom-cavity interaction time $2\pi/g \sim 20 \mu\text{s}$. Note that optical cavities with a high $Q \sim 10^{10}$ or greater have been demonstrated in experiments [77,78]. Thus, the present proposal might be realizable using current cavity QED setups.

VII. CONCLUSION

We have presented an efficient method to realize an n-qubit controlled phase gate or an n-qubit Toffoli gate with n qubits distributed in different cavities. As shown above, the method has the following advantages: (i) Only one auxiliary qutrit is used to couple the cavities and no other auxiliary system is required, thus the hardware resources is significantly reduced; (ii) The gate implementation is deterministic since no measurement is needed; (iii) The gate can in principle be performed fast for a small number of qubits, because of only employing resonant interaction; and (iv) By using the conventional gate-decomposing protocols to construct the multi-control-qubit gate, the number of required basic gates (single-qubit or two-qubit gates) drastically increases as the number of qubits increases. In a stark contrast, as shown above, the number of basic operations, required by our proposal, only increases *linearly* with the number of qubits. Thus, the gate realization by this proposal is greatly simplified when compared to using conventional gate decomposing protocols.

We have further investigated the experimental feasibility of implementing the proposed gate for a three-qubit case, based on circuit QED. Numerical simulations show that high-fidelity implementation of a three-qubit controlled phase gate, which is executed on three qubits distributed in three different cavities, is feasible within current circuit QED technology. The method is quite general and can be applied to realize the proposed gate with qubits distributed in different cavities, in various physical systems, such as natural atoms or artificial atoms (e.g., quantum dots, NV centers, various superconducting qutrits, etc.) distributed in different cavities.

Finally, it is noted that the method can be applied to implement a multiqubit controlled phase gate with atoms and a single cavity. As an example, we have explicitly shown how to realize a three-qubit controlled phase gate by loading atoms into or moving atoms out of the cavity, and have analyzed the experimental feasibility.

Before ending conclusion, we should mention that the architecture illustrated in Fig. 1 or Fig. 2(a) would offer more flexibility for a circuit-QED system, when compared with a cavity-QED system consisting of atoms and optical cavities. For atoms, adjusting the atomic level spacings is usually difficult and slow in practice, and loading an atom into more than one cavity simultaneously is challenging and has not been reported in experiments. Also, the speed of adjusting the frequency of an optical cavity is quite slow in experiments. In contrast, as discussed previously, the level spacings of superconducting qutrits can be rapidly adjusted within a few nanoseconds, and the frequency of a microwave cavity or resonator can be quickly tuned in 1–3 ns. In addition, the ancillary superconducting qutrit can be used to couple cavities or resonators via capacitors. By combining these degrees of freedom, several types of important couplings can be achieved, such as: (i) the coupling of the ancillary qutrit with the selective cavities; (ii) the coupling between the selective cavities; and (iii) the coupling among qubits distributed in different cavities. These couplings are necessary in quantum gate implementation, entanglement generation, and quantum state transfer with photonic qubits or superconducting qubits distributed in different cavities, which are of importance in large-scale quantum information processing based on a multi-cavity circuit QED system.

ACKNOWLEDGMENTS

This work was supported in part by the NKRDP of China (Grant No. 2016YFA0301802), the National Natural Science Foundation of China under Grant Nos. [11074062, 11374083, 11774076], and the Zhejiang Natural Science Foundation under Grant No. LZ13A040002. This work was also supported by the funds from Hangzhou City for the

-
- [1] M. A. Nielsen and I. L. Chuang, *Quantum Computation and Quantum Information* Cambridge University Press, Cambridge, England, 2001, p. 182.
- [2] A. Barenco *et al.*, Elementary gates for quantum computation, *Phys. Rev. A* **52**, 3457 (1995).
- [3] C. Jones, Composite Toffoli gate with two-round error detection, *Phys. Rev. A* **87**, 052334 (2013).
- [4] C. P. Yang, Y. X. Liu, and F. Nori, Phase gate of one qubit simultaneously controlling n qubits in a cavity, *Phys. Rev. A* **81**, 062323 (2010).
- [5] P. W. Shor, In Proceedings of the 35th annual symposium on foundations of computer science, edited by S. Goldwasser (IEEE Computer Society Press, Los Alamitos, CA), pp. 124–134 (1994).
- [6] L. K. Grover, Quantum computers can search rapidly by using almost any transformation, *Phys. Rev. Lett.* **80**, 4329 (1998).
- [7] T. Beth and M. Rötteler, *Quantum Information* (Springer, Berlin), Vol. 173, Ch. 4, p. 96 (2001).
- [8] P. W. Shor, Scheme for reducing decoherence in quantum computer memory, *Phys. Rev. A* **52**, R2493 (1995).
- [9] A. M. Steane, Error correcting codes in quantum theory, *Phys. Rev. Lett.* **77**, 793 (1996).
- [10] F. Gaitan, Quantum error correction and fault tolerant quantum computing (CRC Press, USA), pp. 1–312 (2008).
- [11] S. L. Braunstein, V. Bužek, and M. Hillery, Quantum-information distributors: quantum network for symmetric and asymmetric cloning in arbitrary dimension and continuous limit, *Phys. Rev. A* **63**, 052313 (2001).
- [12] M. Šašura and V. Bužek, Multiparticle entanglement with quantum logic networks: application to cold trapped ions, *Phys. Rev. A* **64**, 012305 (2001).
- [13] M. Mötönen, J. J. Vartiainen, V. Bergholm, and M. M. Salomaa, Quantum circuits for general multiqubit gates, *Phys. Rev. Lett.* **93**, 130502 (2004).
- [14] V. V. Shende and I. L. Markov, On the CNOT-cost of TOFFOLI gates, *Quant. Inf. Comp.* **9** (5-6), 461 (2009).
- [15] J. K. Pachos and P. L. Knight, Quantum Computation with a One-Dimensional Optical Lattice, *Phys. Rev. Lett.* **91**, 107902 (2003).
- [16] H. Ollivier and P. Milman, Proposal for realization of a Toffoli gate via cavity-assisted collision, quant-ph/0306064.
- [17] J. Zhang, W. Liu, Z. Deng, Z. Lu, and G. L. Long, Modularization of multi-qubit controlled phase gate and its NMR implementation, *J. Opt. B: Quantum Semiclass. Opt.* **7**, 22(2005).
- [18] A. Fedorov, L. Steffen, M. Baur, da SilvaMP, and A. Wallraff, Implementation of a Toffoli gate with superconducting circuits, *Nature* **481**, 170 (2012).
- [19] L. M. Duan, B. Wang, and H. J. Kimble, Robust quantum gates on neutral atoms with cavity-assisted photon-scattering, *Phys. Rev. A* **72**, 032333 (2005).
- [20] X. Wang, A. Sørensen, and K. Mølmeret, Multibit gates for quantum computing, *Phys. Rev. Lett.* **86**, 3907 (2001).
- [21] X. Zou, Y. Dong, and G. C. Guo, Implementing a conditional z gate by a combination of resonant interaction and quantum interference, *Phys. Rev. A* **74**, 032325 (2006).
- [22] C. P. Yang and S. Han, n -qubit-controlled phase gate with superconducting quantum-interference devices coupled to a resonator, *Phys. Rev. A* **72**, 032311 (2005).
- [23] C. P. Yang and S. Han, Realization of an n -qubit controlled- U gate with superconducting quantum interference devices or atoms in cavity QED, *Phys. Rev. A* **73**, 032317 (2006).
- [24] W. L. Yang, Z. Q. Yin, Z. Y. Xu, M. Feng, and J. F. Du, One-step implementation of multi-qubit conditional phase gating with nitrogen-vacancy centers coupled to a high-Q silica microsphere cavity, *Appl. Phys. Lett.* **96**, 241113 (2010).
- [25] T. Monz *et al.*, Realization of the quantum Toffoli gate with trapped ions, *Phys. Rev. Lett.* **102**, 040501 (2009).
- [26] H. R. Wei and F. G. Deng, Universal quantum gates for hybrid systems assisted by quantum dots inside double-sided optical microcavities, *Phys. Rev. A* **87**, 022305 (2013).
- [27] H. W. Wei and F. G. Deng, Scalable quantum computing based on stationary spin qubits in coupled quantum dots inside double-sided optical microcavities, *Sci. Rep.* **4**, 7551 (2014).
- [28] M. Hua, M. J. Tao, and F. G. Deng, Universal quantum gates on microwave photons assisted by circuit quantum electrodynamics, *Phys. Rev. A* **90**, 012328 (2014).
- [29] M. Hua, M. J. Tao, and F. G. Deng, Fast universal quantum gates on microwave photons with all-resonance operations in circuit QED, *Scientific Reports* **5**, 9274 (2015).
- [30] C. P. Yang, S. B. Zheng, and F. Nori, Multiqubit tunable phase gate of one qubit simultaneously controlling n qubits in a cavity, *Phys. Rev. A* **82**, 062326 (2010).
- [31] C. P. Yang, Q. P. Su, F. Y. Zhang, and S. B. Zheng, Single-step implementation of a multiple-target-qubit controlled phase gate without need of classical pulses, *Opt. Lett.* **39**, 3312 (2014).
- [32] H. F. Wang, A. D. Zhu, and S. Zhang, One-step implementation of a multiqubit phase gate with one control qubit and multiple target qubits in coupled cavities, *Optics Letters* **39**, 1489 (2014).
- [33] T. Liu, X. Z. Cao, Q. P. Su, S. J. Xiong, and C. P. Yang, Multi-target-qubit unconventional geometric phase gate in a multicavity system, *Scientific Reports* **6**, 21562 (2016).
- [34] J. Clarke and F. K. Wilhelm, Superconducting quantum bits, *Nature* **453**, 1031 (2008).
- [35] M. Neeley *et al.*, Process tomography of quantum memory in a Josephson-phase qubit coupled to a two-level state, *Nat.*

- Phys. **4**, 523 (2008).
- [36] P. J. Leek *et al.*, Using sideband transitions for two-qubit operations in superconducting circuits, Phys. Rev. B **79**, 180511(R) (2009).
- [37] J. D. Strand *et al.*, First-order sideband transitions with flux-driven asymmetric transmon qubits, Phys. Rev. B **87**, 220505(R) (2013).
- [38] Z. L. Xiang, X. Y. Lü, T. F. Li, J. Q. You, and F. Nori, Hybrid quantum circuit consisting of a superconducting flux qubit coupled to a spin ensemble and a transmission-line resonator, Phys. Rev. B **87**, 144516 (2013).
- [39] P. Neumann, R. Kolesov, V. Jacques, J. Beck, J. Tisler, A. Batalov, L. Rogers, N. B. Manson, G. Balasubramanian, F. Jelezko, and J. Wrachtrup, Excited-state spectroscopy of single NV defects in diamond using optically detected magnetic resonance, New J. Phys. **11**, 013017 (2009).
- [40] P. Pradhan, M. P. Anantram, and K. L. Wang, Quantum computation by optically coupled steady atoms/quantum-dots inside a quantum electro-dynamic cavity, arXiv:quant-ph/0002006
- [41] M. Sandberg, C. M. Wilson, F. Persson, T. Bauch, G. Johansson, V. Shumeiko, T. Duty, and P. Delsing, Tuning the field in a microwave resonator faster than the photon life time, Appl. Phys. Lett. **92**, 203501 (2008).
- [42] Z. L. Wang, Y. P. Zhong, L. J. He, H. Wang, J. M. Martinis, A. N. Cleland, and Q. W. Xie, Quantum state characterization of a fast tunable superconducting resonator, Appl. Phys. Lett. **102**, 163503 (2013).
- [43] Y. Yang and S. Han, private communication
- [44] C. P. Yang, Q. P. Su, S. B. Zheng, F. Nori, and S. Han, Entangling two oscillators with arbitrary asymmetric initial states. Phys. Rev. A **95**, 052341 (2017)
- [45] C. P. Yang, S. I. Chu, and S. Han, Possible realization of entanglement, logical gates and quantum information transfer with superconducting-quantum-interference-device qubits in cavity QED, Phys. Rev. A **67**, 042311 (2003).
- [46] J. Q. You and F. Nori, Quantum information processing with superconducting qubits in a microwave field, Phys. Rev. B **68**, 064509 (2003).
- [47] A. Blais, R. S. Huang, A. Wallraff, S. M. Girvin, and R. J. Schoelkopf, Cavity quantum electrodynamics for superconducting electrical circuits: An architecture for quantum computation, Phys. Rev. A **69**, 062320 (2004).
- [48] J. Q. You and F. Nori, Superconducting circuits and quantum information, Phys. Today **58**, 42 (2005).
- [49] J. Q. You and F. Nori, Atomic physics and quantum optics using superconducting circuits, Nature **474**, 589 (2011).
- [50] I. Buluta, S. Ashhab, and F. Nori, Natural and artificial atoms for quantum computation, Rep. Prog. Phys. **74**, 104401 (2011).
- [51] Z. L. Xiang, S. Ashhab, J. Q. You, and F. Nori, Hybrid quantum circuits: Superconducting circuits interacting with other quantum systems, Rev. Mod. Phys. **85**, 623 (2013).
- [52] X. Gu, A. F. Kockum, A. Miranowicz, Y. X. Liu, and F. Nori, Microwave photonics with superconducting quantum circuits. Phys. Rep. **718-719**, pp. 1-102 (2017).
- [53] M. Khezri, E. Mlinar, J. Dressel, and A. N. Korotkov, Measuring a transmon qubit in circuit QED: dressed squeezed states, Phys. Rev. A **94**, 012347 (2016).
- [54] Z. B. Feng, Quantum state transfer between hybrid qubits in a circuit QED, Phys. Rev. A **85**, 014302 (2012).
- [55] S. Aldana, Y. D. Wang, and C. Bruder, Greenberger-Horne-Zeilinger generation protocol for N superconducting transmon qubits capacitively coupled to a quantum bus, Phys. Rev. B **84**, 134519 (2011).
- [56] Y. X. Liu, L. F. Wei, and F. Nori, Generation of nonclassical photon states using a superconducting qubit in a microcavity, Europhys. Lett. **67**, 941 (2004).
- [57] Z. B. Feng, Coupling charge qubits via Raman transitions in circuit QED, Phys. Rev. A **78**, 032325 (2008).
- [58] Y. D. Wang, S. Chesi, D. Loss, and C. Bruder, One-step multiqubit Greenberger-Horne-Zeilinger state generation in a circuit QED system, Phys. Rev. B **81**, 104524 (2010).
- [59] C. P. Yang, Q. P. Su, S. B. Zheng, and F. Nori, Crosstalk-insensitive method for simultaneously coupling multiple pairs of resonators, Phys. Rev. A **93**, 042307 (2016).
- [60] T. Niemczyk, F. Deppe, H. Huebl, E. P. Menzel, F. Hocke, M. J. Schwarz, J. J. Garcia-Ripoll, D. Zueco, T. Hummer, and E. Solano *et al.*, Circuit quantum electrodynamics in the ultrastrong-coupling regime, Nat. Phys. **6**, 772 (2010).
- [61] L. DiCarlo *et al.*, Preparation and measurement of three-qubit entanglement in a superconducting circuit, Nature **467**, 574 (2010)
- [62] M. Baur, S. Filipp, R. Bianchetti, J. M. Fink, M. Göppl, L. Steffen, P. J. Leek, A. Blais, and A. Wallraff, Measurement of Autler-Townes and Mollow Transitions in a Strongly Driven Superconducting Qubit, Phys. Rev. Lett. **102**, 243602 (2009).
- [63] J. Koch, T. M. Yu, J. Gambetta, A. A. Houck, D. I. Schuster, J. Majer, A. Blais, M. H. Devoret, S. M. Girvin, and R. J. Schoelkopf, Charge-insensitive qubit design derived from the Cooper pair box, Phys. Rev. A **76**, 042319 (2007).
- [64] C. Rigetti, J. M. Gambetta, S. Poletto, B. L. T. Plourde, J. M. Chow, A. D. Córcoles, J. A. Smolin, S. T. Merkel, J. R. Rozen, G. A. Keefe *et al.*, Superconducting qubit in a waveguide cavity with a coherence time approaching 0.1 ms, Phys. Rev. B **86**, 100506(R) (2012).
- [65] J. B. Chang *et al.*, Improved superconducting qubit coherence using titanium nitride, Appl. Phys. Lett. **103**, 012602 (2013)
- [66] J. M. Chow *et al.*, Implementing a strand of a scalable fault-tolerant quantum computing fabric, Nat. Commun. **5**, 4015 (2014)
- [67] I. M. Pop, K. Geerlings, G. Catelani, R. J. Schoelkopf, L. I. Glazman, and M. H. Devoret, Coherent suppression of electromagnetic dissipation due to superconducting quasiparticles, Nature **508**, 369 (2014).
- [68] C. P. Yang, Q. P. Su, and S. Han, Generation of Greenberger-Horne-Zeilinger entangled states of photons in multiple cavities via a superconducting qubit or an atom through resonant interaction, Phys. Rev. A **86**, 022329 (2012)
- [69] C. P. Yang, Q. P. Su, and F. Nori, Entanglement generation and quantum information transfer between spatially-separated

- qubits in different cavities, *New J. Phys.* **15**, 115003 (2013).
- [70] W. Chen, D. A. Bennett, V. Patel, and J. E. Lukens, Substrate and process dependent losses in superconducting thin film resonators, *Supercond. Sci. Technol.* **21**, 075013 (2008).
- [71] P. J. Leek, M. Baur, J. M. Fink, R. Bianchetti, L. Steffen, S. Filipp, and A. Wallraff, Cavity quantum electrodynamics with separate photon storage and qubit readout modes, *Phys. Rev. Lett.* **104**, 100504 (2010).
- [72] L. Steffen, Y. Salathe, M. Oppliger, P. Kurpiers, M. Baur, C. Lang, C. Eichler, G. Puebla-Hellmann, A. Fedorov, and A. Wallraff, Deterministic quantum teleportation with feed-forward in a solid state system, *Nature* **500**, 319 (2013).
- [73] K. M. Fortier, S. Y. Kim, M. J. Gibbons, P. Ahmadi, and M. S. Chapman, Deterministic Loading of Individual Atoms to a High-Finesse Optical Cavity, *Phys. Rev. Lett.* **98**, 233601 (2007).
- [74] M. Khudaverdyan, W. Alt, I. Dotsenko, T. Kampschulte, K. Lenhard, A. Rauschenbeutel, S. Reick, K. Schörner, A. Widera, and D. Meschede, Controlled insertion and retrieval of atoms coupled to a high-finesse optical resonator, *New J. Phys.* **10**, 073023 (2008).
- [75] M. Brune, E. Hagley, J. Dreyer, X. Maitre, A. Maali, C. Wunderlich, J. M. Raimond, and S. Haroche, Observing the Progressive Decoherence of the “Meter” in a Quantum Measurement, *Phys. Rev. Lett.* **77**, 4887 (1996).
- [76] S. Osnaghi, P. Bertet, A. Auffeves, P. Maioli, M. Brune, J. M. Raimond, and S. Haroche, Coherent Control of an Atomic Collision in a Cavity, *Phys. Rev. Lett.* **87**, 037902 (2001).
- [77] S. Kuhr, S. Gleyzes, C. Guerlin, J. Bernu, U. B. Hoff, S. Deléglise, S. Osnaghi, M. Brune, and J.-M. Raimond, Ultrahigh finesse Fabry-Pérot superconducting resonator, *Appl. Phys. Lett.* **90**, 164101 (2007).
- [78] G. Rempe, F. SchmidtKaler, H. Walther, Observation of sub-Poissonian photon statistics in a micromaser, *Phys. Rev. Lett.* **64**, 2783 (1990).